

Return of your e-proof to AMS signifies that you have thoroughly read and approve of the proof, and thereby authorize publication based on the proof (except where you have identified errors or indicated desired changes within the proof file, or clearly itemized these changes in the email to pdfproofs@ametsoc.org).

Return of the e-proof also signifies agreement to pay all publication charges (except for cases where a waiver has been granted).

Adjustments for AMS style may be made prior to publication.

Proofreading

The most efficient (and highly encouraged) way to correct the page proofs and return them to AMS is to electronically annotate the PDF file containing your proof **using the annotation tools** described below in Adobe Acrobat and **send it via e-mail to pdfproofs@ametsoc.org**. Instructions for the PDF annotation process appear on the following pages. If necessary, you may instead print out your page proofs, make your corrections on the pages, and fax or express mail them to AMS. The fax number and delivery address are located at the end of this document.

Proofread the proofs carefully, as this will be your only chance to see your article before publication. **Pay special attention to color figures (if any), and characters such as Greek letters and mathematical symbols.** Make sure that everything is typeset the way that you want it as the corrected proofs will not be returned to you.

Alterations

Answer author queries at the appropriate place in the text and correct any errors you find. **Authors are allowed up to 10 new textual edits at proof stage at no additional charge** (copy and technical editing errors are not charged to authors at any time). **Additional edits will be charged at the rate of \$4.50 per edit, and changes to figures are more expensive (~\$20 per black and white figure and ~\$30-\$50 per color figure).**

The layout in the page proof is considered final unless changes are essential. Every effort should be made to balance text and figure alterations so that deletions are compensated by nearby additions, and figure substitutions should be of the same size and shape, if possible. Please also note that material changes to the *science* in the manuscript at this stage will require further peer review, substantially increasing the time to publication. **The editors reserve the right to accept or reject proposed alterations.**

Figures

The figures that appear in your page proofs are lower resolution than the final printed article. The primary AMS technical editor for your journal will be reviewing figure quality prior to publication. If you have specific concerns about any of your figures, especially if any color figures do not appear in color, please describe them in your return. Please verify that each figure properly corresponds with the figure captions and citations in the text. If there are corrections that need to be made, send a new electronic version in eps or tiff format of the corrected figure with your corrected proofs. Include your name, the figure number, and the manuscript number.

Reprints

If you would like to order hard-copy reprints in addition to the complimentary pdf, please use the reprint order form (available at <http://www.ametsoc.org/PUBS/journals/reprintorder.pdf>).

Thank you very much for your cooperation, and thank you for publishing with the AMS.

Lauren Foster
American Meteorological Society
45 Beacon St.
Boston, MA 02108-3693
Fax: (617) 973-0468

Annotating PDFs



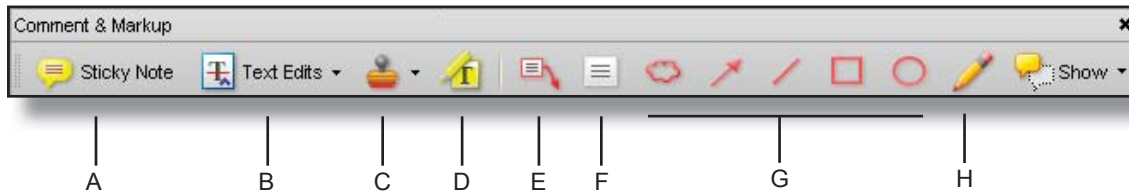
ams_annotating_pdfs1.1; April 09, 2009; full release

1. Introduction

eProof files are self-contained PDF documents for viewing on-screen and for printing. They contain all appropriate formatting and fonts to ensure correct rendering on-screen and when printing hardcopy. DJS sends eProofs that can be viewed, annotated, and printed using the free version of Acrobat Reader 7 (or greater). These eProofs are “enabled” with commenting rights, therefore they can be modified by using special markup tools in Acrobat Reader that are not normally available unless using the Standard or Professional version.

The screen images in this document were captured on a PC running Adobe Acrobat Reader version 8.1.0. Though some of the images may differ in appearance from your platform/version, basic functionality remains similar. At the time of this writing, Acrobat Reader v9.1 is freely available and can be downloaded from: <http://get.adobe.com/reader/>

2. Comment & Markup toolbar functionality



A. Sticky Note tool; B. Text Edits tool; C. Stamp tool; D. Highlight Text tool; E. Callout tool; F. Text Box tool; G. Various Object tools; H. Pencil tool

A. Show the Comment & Markup toolbar

The Comment & Markup toolbar doesn't appear by default. Do one of the following:

- Select View > Toolbars > Comment & Markup.
- Select Tools > Comment & Markup > Show Comment & Markup Toolbar.
- Click the Review & Comment button in the Task toolbar, and choose Show Comment & Markup Toolbar.

To add or remove tools for this toolbar, right-click the toolbar and select the tool. Or, select Tools > Customize Toolbars.

B. Select a commenting or markup tool

Do one of the following:

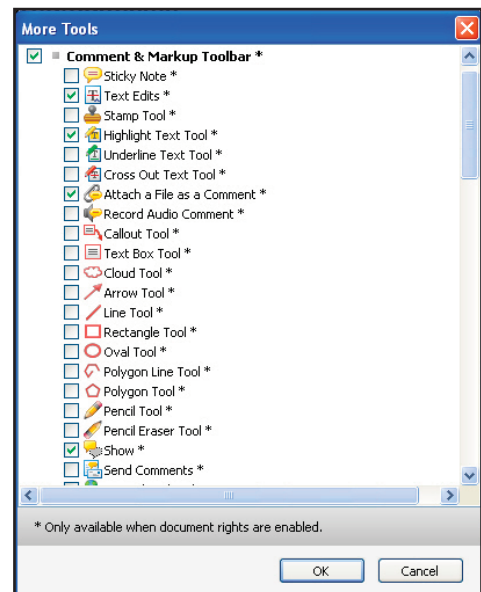
- Select a tool from the Comment & Markup toolbar.
- Select Tools > Comment & Markup > [tool].

Note: After an initial comment is made, the tool changes back to the Select tool so that the comment can be moved, resized, or edited. (The Pencil, Highlight Text, and Line tools stay selected.)

C. Keep a commenting tool selected

Multiple comments can be added without reselecting the tool. Select the tool to use (but don't use it yet).

- Select View > Toolbars > Properties Bar.
- Select Keep Tool Selected.



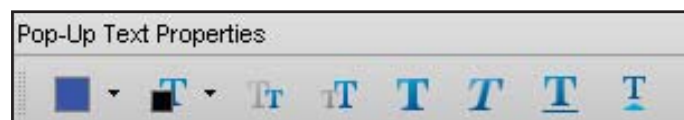
Choose Tools > Customize Toolbars to remove unnecessary items from the toolbar (see Section 7 for suggested toolbar layout)

3. The Properties bar


The Properties bar can be used to format text and select options for individual tools.

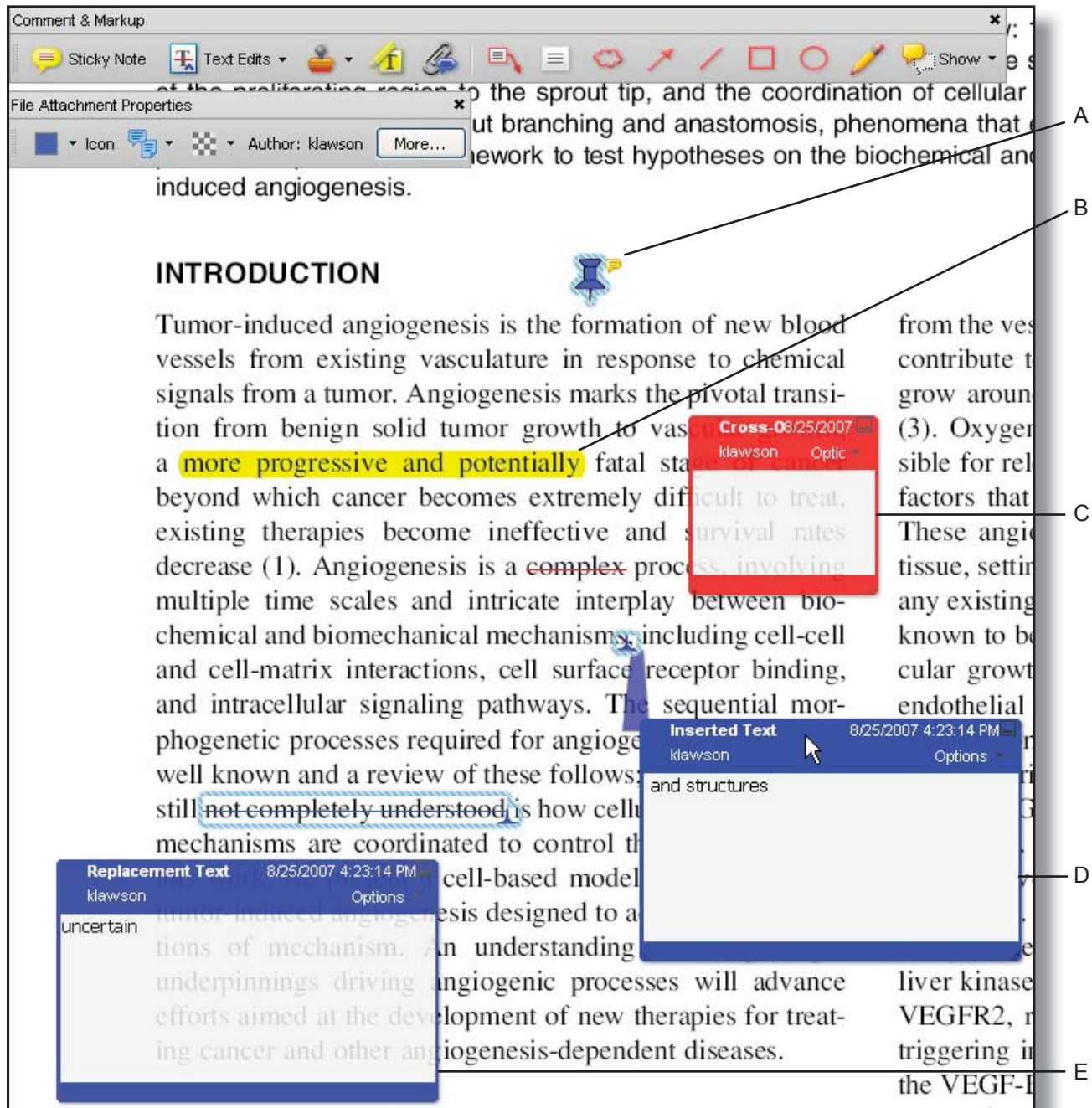
To view the Properties bar, do one of the following:

- Choose View > Toolbars > Properties Bar.
- Right-click the toolbar area; choose Properties Bar.
- Select [Ctrl-E]



4. Using the comment and markup tools

To *insert*, *delete*, or *replace* text, use the **Text Edits** tool. Select the Text Edits tool, then select the text with the cursor (or simply position it) and begin typing. A pop-up note will appear based upon the modification (e.g., inserted text, replacement text, etc.). Use the Properties bar to format text in pop-up notes. A pop-up note can be minimized by selecting the  button inside it.



A. Attached file; B. Highlighted text; C. Crossed-out (strike-through) text; D. Inserted text; E. Replaced text

5. Inserting symbols or special characters

An 'insert symbol' feature is not available for annotations, and copying/pasting symbols or non-keyboard characters from Microsoft Word does not always work. Use angle brackets < > to indicate these special characters (e.g., <alpha>, <beta>).

6. Editing near watermarks and hyperlinked text

eProof documents often contain watermarks and/or hyperlinked text. Selecting characters near these items can be difficult using the mouse alone. To edit an eProof which contains text in these areas, do the following:

- Without selecting the watermark or hyperlink, place the cursor near the area for editing.
- Use the arrow keys to move the cursor beside the text to be edited.
- Hold down the shift key while simultaneously using arrow keys to select the block of text, if necessary.
- Insert, replace, or delete text, as needed.

7. Summary of main functions

Insert text - Use Text Edits tool (position cursor and begin typing)

Replace text - Use Text Edits tool (select text and begin typing)

Delete text - Use Text Edits tool (select text and press delete key)

Highlight text - Use Highlight Text tool (select text)

Attach a file - Use the Attach a File with Comment tool (select tool, position cursor and click mouse, select file)



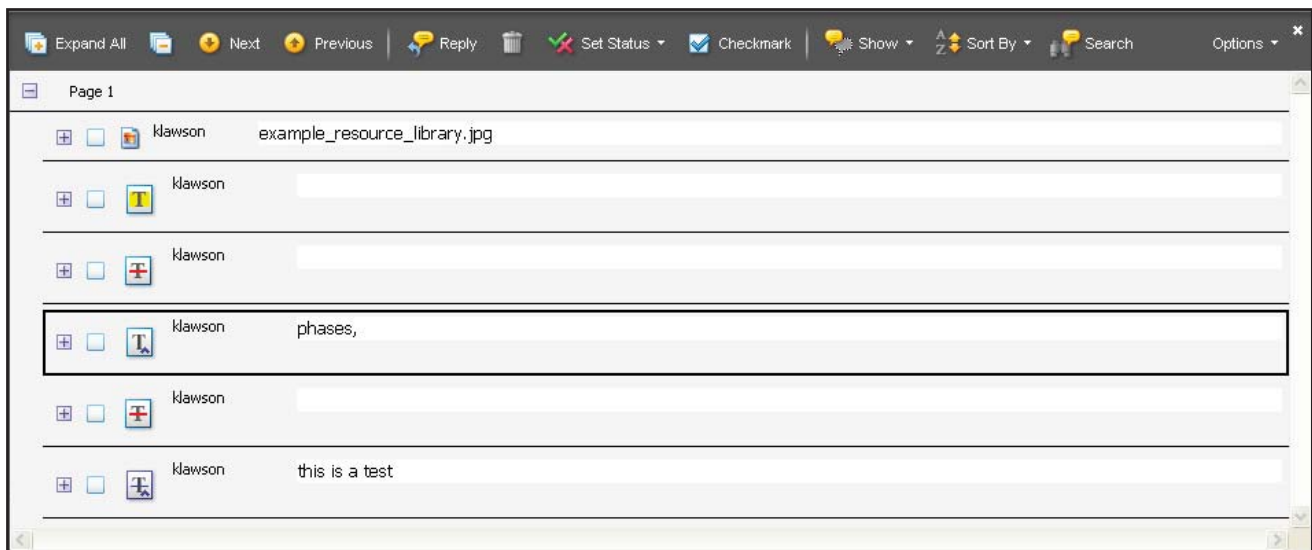
Suggested toolbar layout

8. Reviewing changes

To review all changes, do the following:

- Select the Show button on the Comment & Markup toolbar.
- Select Show Comments List.

Note: Selecting a correction in the list will highlight the corresponding item in the document, and vice versa.



Use the Comments list to review all changes

NUMBER 1 OF 1

AUTHOR QUERIES

DATE 6/24/2010

JOB NAME JPO

JOB NUMBER 0

ARTICLE jpo4324

QUERIES FOR AUTHORS ARDHUIN ET AL.

PLEASE ANSWER THE AUTHOR QUERIES WHERE THEY APPEAR IN THE TEXT.

AU1: Please note for future submissions that citations are not allowed in the abstract per AMS style. Please check edits.

AU2: Have Parts II and/or III of this paper been submitted for publication?

AU3: Should the “[“ after the 2π be “[”]

AU4: What is u^* ?

AU5: For Arduin et al. (2008a) who sponsored this meeting?

AU6: For Bidlot et al. (2005) please provide the total page count.

AU7: For Bidlot et al. (2007a) please provide the total page count.

AU8: For Bidlot et al. (2007b) please provide the page range or paper ID number.

AU9: For Filipot et al. (2010) please update the status of this article.

AU10: For Lefevre et al. (2004) please provide the page range or paper ID number.

AU11: For Makin and Stam (2003) please provide the total page count.

AU12: For Tolman (2009) please provide the total page count.

AU13: For Tsagareli (2008) please provide the total page count.

AU14: For Arduin et al. (2009), please indicate if this should be (2009a), (2009b), or (2009a,b).

AU15: Where is the description for the top left panel?

AU16: Please define SIN3.

AU17: Chalikov, D. V., 1993 is mismatched with intext citations. Please confirm.

Semiempirical Dissipation Source Functions for Ocean Waves. Part I: Definition, Calibration, and Validation

FABRICE ARDHUIN,^{*} ERICK ROGERS,⁺ ALEXANDER V. BABANIN,[#] JEAN-FRANÇOIS FILIPOT,[@]
RUDY MAGNE,[@] AARON ROLAND,[&] ANDRE VAN DER WESTHUYSEN,^{**} PIERRE QUEFFEULOUN,^{*}
JEAN-MICHEL LEFEVRE,⁺⁺ LOTFI AOUF,⁺⁺ AND FABRICE COLLARD^{##}

^{*} Laboratoire d'Océanographie Spatiale, Ifremer, Plouzané, France

⁺ Oceanography Division, Naval Research Laboratory, Stennis Space Center, Mississippi

[#] Swinburne University, Hawthorn, Victoria, Australia

[@] Service Hydrographique et Océanographique de la Marine, Brest, France

& Technological University of Darmstadt, Darmstadt, Germany

^{**} Delft, Delft, Netherlands

⁺⁺ UMR GAME, Météo-France-CNRS, Toulouse, France

^{##} Radar Division, CLS, Plouzané, France

(Manuscript received 27 July 2009, in final form 26 March 2010)

AUI



ABSTRACT

New parameterizations for the spectral dissipation of wind-generated waves are proposed. The rates of dissipation have no predetermined spectral shapes and are functions of the wave spectrum and wind speed and direction, in a way consistent with observations of wave breaking and swell dissipation properties. Namely, the swell dissipation is nonlinear and proportional to the swell steepness, and dissipation due to wave breaking is nonzero only when a nondimensional spectrum exceeds the threshold at which waves are observed to start breaking. An additional source of short-wave dissipation is introduced to represent the dissipation of short waves due to longer breaking waves. A reduction of the wind-wave generation of short waves is meant to account for the momentum flux absorbed by longer waves. These parameterizations are combined and calibrated with the discrete interaction approximation for the nonlinear interactions. Parameters are adjusted to reproduce observed shapes of directional wave spectra, and the variability of spectral moments with wind speed and wave height. The wave energy balance is verified in a wide range of conditions and scales, from the global ocean to coastal settings. Wave height, peak and mean periods, and spectral data are validated using in situ and remote sensing data. Some systematic defects are still present, but, overall, the parameterizations probably yield the most accurate estimates of wave parameters to date. Perspectives for further improvement are also given.

1. Introduction

a. On phase-averaged models

Spectral wave modeling has been performed for the last 50 years, using the wave energy balance equation (Gelci et al. 1957). This model is based on a spectral decomposition of the surface elevation variance across wavenumbers k and directions θ . The spectra density F evolves in five dimensions that are the two spectral dimensions k and θ , the two physical dimensions of the ocean surface (usually longitude and latitude), and time t :

$$\frac{dF}{dt} = S_{\text{atm}} + S_{\text{nl}} + S_{\text{oc}} + S_{\text{bt}}, \quad (1)$$

where the Lagrangian derivative is the rate of change of the spectral density following a wave packet at its group speed in both physical and spectral spaces. In particular, this spectral advection includes changes in direction due to the earth's sphericity, as well as refraction over varying topography (e.g., Munk and Traylor 1947; Magne et al. 2007) and currents, and changes in wavelength or period in similar conditions (Barber 1949).

The spectral source functions on the right-hand side of Eq. (1) are grouped into their atmospheric (S_{atm}), nonlinear scattering (S_{nl}), oceanic (S_{oc}), and bottom (S_{bt}) sources. This grouping, like any other, is largely arbitrary. For example, waves that break are nonlinear. Thus, the

Corresponding author address: Fabrice Ardhuin, Laboratoire d'Océanographie Spatiale, Ifremer, 29200 Plouzané, France.
E-mail: ardhuin@shom.fr

effects of breaking waves, which are contained in S_{oc} , is intrinsically related to the nonlinear evolution term contained in S_{nl} . Yet, compared to the usual separation of deep-water evolution by wind input, nonlinear interactions, and dissipation (e.g., WAMDI Group 1988), this grouping has the benefit of identifying where the energy and momentum are going to or coming from, which is a necessary feature when ocean waves are used to drive or are coupled with atmospheric or oceanic circulation models (e.g., Janssen et al. 2004; Ardhuin et al. 2008b).

Here, S_{atm} , which gives the flux of energy from the atmospheric nonwave motion to the wave motion, is the sum of a wave generation term S_{in} and a wind-generation term S_{out} (often referred to as negative wind input, i.e., a wind output). The nonlinear scattering term S_{nl} represents all processes that lead to an exchange of wave energy between the different spectral components. In deep and intermediate water depth, this is dominated by cubic interactions between quadruplets of wave trains, while quadratic nonlinearities play an important role in shallow water (e.g., WISE Group 2007). The ocean source S_{oc} may accommodate wave–current interactions¹ and interactions of surface and internal waves. The oceanic source term S_{oc} is restricted to wave breaking and wave–turbulence interactions.

The basic principle underlying Eq. (1) is that waves essentially propagate as a superposition of almost linear wave groups that evolve on longer time scales as a result of weak-in-the-mean processes (e.g., Komen et al. 1994). Recent reviews have questioned the possibility of further improving numerical wave models without changing this basic principle (Cavaleri 2006). Although this may be true in the long term, we demonstrate here that it is possible to improve our model results significantly by including more physical features in the source term parameterizations. The main advance that we propose is the adjustment of a dissipation function without any prescribed spectral shape, based on our empirical knowledge of the breaking of random waves (Banner et al. 2000; Babanin et al. 2001) and the dissipation of swells over long distances (Ardhuin et al. 2009a). The present formulations are ~~still semiempirical, in the sense that they are~~ not based on a detailed physical model of dissipation processes, but they demonstrate that progress is possible. This effort opens the way for physical parameterizations (e.g., Filipot et al. 2010) that will eventually provide new applications for wave models, such as the estimation of statistical parameters for breaking waves, including

whitecap coverage and foam thickness. Other efforts, though less empirical in nature, are also under way to arrive at better parameterizations (e.g., Banner and Morison 2006; Babanin et al. 2007; Tzagareli 2008), but they have yet to produce a practical alternative for wave forecasting and hindcasting.

b. Shortcomings of existing parameterizations

Until the work of van der Westhuysen et al. (2007), none of the wave dissipation parameterizations presented in the literature had a quantitative relationship with observed features of wave dissipation but rather they were adjusted to close the wave energy balance. Komen et al. (1984) have produced a family of parameterizations loosely justified by the “random pulse” theory of Hasselmann (1974). In deep water, parameterizations take a generic form:

$$S_{oc}(k, \theta) = C_{ds} g^{0.5} k_r^{4.5} H_s^4 \left[\delta_1 \frac{k}{k_r} + \delta_2 \left(\frac{k}{k_r} \right)^2 \right] F(k, \theta), \quad (2)$$

in which C_{ds} is a negative constant, $F(k, \theta)$ is the spectral density, and $H_s = 4 \sqrt{\iint E(k, \theta) dk d\theta}$ is the significant wave height. The energy-weighted mean wavenumber k_r is defined from the entire spectrum as follows:

$$k_r = \left[\frac{16}{H_s^2} \int_0^{f_{max}} \int_0^{2\pi} k^r E(k, \theta) dk d\theta \right]^{1/r}, \quad (3)$$

where r is a real constant. Usual choices are $r = -0.5$ (WAMDI Group 1988) or $r = 0.5$ (Komen et al. 1984; Bidlot et al. 2005).

These parameterizations are still widely used in spite of inconsistencies in the underlying theory. Indeed, if whitecaps do act as random pressure pulses, their average work on the underlying waves only occurs because of a phase correlation between the vertical orbital velocity field and the moving whitecap position, which travels with the breaking wave. In reality the horizontal shear is likely to be the dominant mechanism (Longuet-Higgins and Turner 1974), but the question of correlation remains the same. For any given whitecap, such a correlation cannot exist for all spectral wave components: a whitecap that travels with one wave leads to the dissipation of spectral wave components that propagate in similar directions, with comparable phase velocities. However, whitecaps moving in one direction will give (on average) a zero correlation for waves propagating in the opposite direction because the position of the crests of these opposing waves are completely random with respect to the whitecap position. As a result, not all wave components are dissipated by a given whitecap (others should even be generated), and the dissipation function cannot take the spectral form (2).

¹ In the presence of variable current, the source of energy for the wave field is the work of the radiation stresses. It is not explicit when the energy balance is written as an action balance (e.g., Komen et al. 1994).



A strict interpretation of the pressure pulse model gives a zero dissipation for swells in the open ocean because the swell wave phases are uncorrelated to those of the shorter breaking waves. There is only a negligible dissipation due to short-wave modulations by swells and preferential breaking on the swell crests (Phillips 1963; Hasselmann 1971; Ardhuin and Jenkins 2005). Still, the dissipation functions given by Eq. (2) are applied to the entire spectrum, including swells, without any physical justification.

In spite of its successful use for the estimation of the significant wave height H_s and peak period T_p , these fixed-shape parameterizations, from Komen et al. (1984) up to Bidlot et al. (2007a), have built-in defects that limit the accuracy of the mode results. Most conspicuous is the spurious amplification of wind sea growth in the presence of swell (e.g., van Vledder and Hurdle 2002), which is contrary to all of the observations (Dobson et al. 1989; Violante-Carvalho et al. 2004; Ardhuin et al. 2007). ~~Associated with that defect also comes an underestimation of the energy level in the inertial range, making these wave models ill-suited for remote sensing studies, as will be exposed below.~~

Also, these parameterizations typically give a decreasing dissipation of swell with increasing swell steepness, contrary to all of the observations from Darbyshire (1958) to Ardhuin et al. (2009b). This effect is easily revealed by taking a sea state composed of a swell of energy E_1 and mean wavenumber k_1 and a windsea of energy E_2 and mean wavenumber k_2 , with $k_2 > k_1$. The overall mean wavenumber is

$$k_r = [(k_1^r E_1 + k_2^r E_2)/(E_1 + E_2)]^{1/r}. \quad (4)$$

At low frequency (i.e., small wavenumbers) the dissipation for a given value of k is given by the first term, proportional to $k_r^{3.5}(E_1 + E_2)$. Now, if we keep k_1, k_2 and E_2 constant and only increase the swell energy E_1 , the relative change in dissipation is, according to (2), proportional to $x = 3.5[(k_1/k_r)^r - 1]/r + 2$. For $r = 0.5$, as used by Bidlot et al. (2005, hereinafter BAJ), x is negative (i.e., the dissipation decreases with increasing swell energy) for $k_1/k_r < 0.51$. For equal energy in sea and swell, this occurs when $k_1/k_2 < 0.3$, which is generally the case with sea and swell in the ocean. This erroneous decrease of swell dissipation with increasing swell steepness is reduced when the model frequency range is limited to a maximum frequency of 0.4 Hz, in which case the lowest winds (less than 5 m s^{-1}) are unable to produce a realistic wind sea level, hence limiting the value of k_r to relatively small values.

An alternative and widely used formulation has been proposed by Tolman and Chalikov (1996), and some of

its features are worth noting. We refer to this parameterization as TC, including the later adjustments by Tolman (2002b). It combines two distinct dissipation formulations for high and low frequencies, with a transition at 2 times the wind sea peak frequency. Janssen et al. (1994) had already introduced the use of two terms, k and k^2 in Eq. (2), to represent the different effects in the high- and low-frequency parts of the spectrum. However, both terms are still multiplied by the same factor, $C_{ds} g^{0.5} k_r^{4.5} H_s^4 \delta$. In TC, these two dissipation terms are completely distinct, the low-frequency part being a linear function of the spectral density and proportional to wind friction velocity, u_{*} ; the high-frequency part is also linear and proportional to u_{*}^2 . In this formulation the frequency dependence of the two terms is also prescribed. Tolman and Chalikov (1996) further included swell attenuation by the wind, ~~based on numerical simulations of the airflow above waves (Chalikov and Belevich 1993)~~, here noted S_{out} . At relatively short fetches, the S_{in} and S_{oc} terms in TC are typically a factor of 2–3 times smaller than those of Janssen et al. (1994). This small magnitude of the source terms was found to produce important biases in wave growth and wave directions at short fetch (Ardhuin et al. 2007). Another successful set of parameterizations, for high winds conditions, is the combination by Makin and Stam (2003), but it does not produce accurate results in moderate sea states (Lefèvre et al. 2004). Polnikov and Inocentini (2008) have also proposed new source term formulations, but their results appear to generally be less accurate than those with the model presented here, in particular for mean periods.

Considering the observed strong wave height gradients in rapidly varying currents, Phillips (1984) proposed a dissipation rate proportional to the nondimensional spectrum, also termed the saturation spectrum. Banner et al. (2002) indeed found a correlation of the direction-integrated saturation B with the breaking probability of dominant waves. In particular, they found that breaking occurs when B exceeds a threshold B_r . Alves and Banner (2003) proposed to define the dissipation S_{oc} by B/B_r to some power, multiplied by a Komen-type dissipation term. Although this approach avoided the investigation of the dissipation of nonbreaking waves, it imported all of the above-mentioned defects of that parameterization. Further, their value for B_r , which was much higher than suggested by the observations, tends to disconnect the parameterization from the observed effects (Babanin and van der Westhuysen 2008).

The use of a saturation parameter was taken up again by van der Westhuysen et al. (2007, hereafter WZB). They followed Banner et al. (2002) and integrated the saturation spectrum over directions:

$$B(k) = \int_0^{2\pi} k^3 F(k, \theta') d\theta'. \quad (5)$$

From this, the WZB source function was defined as

$$S_{\text{oc,WZB}}(k, \theta) = C_{\text{ds,WZB}} \sqrt{gk} \left[\frac{B(k)}{B_r} \right]^{p/2} F(k, \theta), \quad (6)$$

where $C_{\text{ds,WZB}}$ is a negative constant, B_r is a constant saturation threshold, and p is a coefficient that varies both with the wind friction velocity u_* and the degree of saturation $B(k)/B_r$ with, in particular, $p \approx 0$ for $B(k) < 0.8B_r$. For nonbreaking waves, when $p \approx 0$, the dissipation is too large by at least one order of magnitude, making the parameterization unfit for oceanic-scale applications, with wave heights in the Atlantic underpredicted by about 50% (Ardhuin and Le Boyer 2006). Van der Westhuysen (2007) eventually replaced this dissipation of nonbreaking waves with the Komen-type form proposed by the WAMDI Group (1988).

Further, the increase in p with the inverse wave age, u_*/C , tends to increase S_{oc} at high frequency, and was needed to obtain a balance with the S_{atm} term in Eq. (1). This indicates that, in addition to the value of the saturation B_r , other factors may be important, such as the directionality of the waves (Banner et al. 2002). Other observations clearly show that the breaking rate of high-frequency waves is much higher for a given value of B , probably due to the cumulative effects by which the longer waves are modifying the dissipation of shorter waves.

Banner et al. (1989) and Melville et al. (2002) have shown that breaking waves suppress the short waves on the surface. Young and Babanin (2006) arrived at the same conclusion from the examination of pre- and post-breaking wave spectra, and proposed a parameterization for S_{oc} that included a new “cumulative term” to represent this effect. Yet, their estimate was derived for very strong wind-forcing conditions only. Their interpretation of the differences in parts of a wave record with breaking and nonbreaking waves implies an underestimation of the dissipation rates because the breaking waves have already lost some energy when they are observed and the nonbreaking waves are not going to break right after they have been observed. Also, since the spectra are different, nonlinear interactions must be different, even on this relatively small time scale (e.g., Young and van Vledder 1993, Fig. 5), and the differences in spectra may not be the result of dissipation alone.

Finally, the recent measurement of swell dissipation by Ardhuin et al. (2009a) has revealed that the dissipation of nonbreaking waves is essentially a function of the wave steepness, and a very important process for ocean

basins larger than 1000 km. Because of the differences in coastal and larger-scale sea states (e.g., Long and Resio 2007), verifying the source function parameterizations at all scales is paramount, in order to provide a robust and comprehensive parameterization of the wave dissipation.

c. A new set of parameterizations

It is thus time to combine the existing knowledge on the dissipation of breaking and nonbreaking waves to assemble a parameterization for the dissipation of waves. Our objective is to provide a robust parameterization that improves on existing wave models. For this we will use the parameterization by BAJ as a benchmark because it was shown to provide the best forecasts on global scales (Bidlot et al. 2007b) before the advent of the parameterizations presented here. BAJ is also fairly close to the widely used Wave Action Model (WAM) “cycle 4” parameterization employed by Janssen and others (Komen et al. 1994).

We will first present a general form of the dissipation terms based on observed wave dissipation features. The degrees of freedom in the parameterization are then used to adjust the model results. A comprehensive validation of wave parameters is then presented using field experiments and a 1-yr hindcast of waves at the global and regional scales, in which all existing wave measurements are considered, with significant wave heights ranging from 0 to 17 m. The model is further validated with independent data at regional and global scales. Model hindcasts and forecasts at global and regional scales are available online (<http://tinyurl.com/yesofy>), covering at least the years 2002–10.

Tests and verification in the presence of currents, and using a more realistic parameterization of wave–wave interactions will be presented in future publications. These may also include some replacement of the arbitrary choices made here.

2. Parameterizations

In this section we present the results of the integration of the energy balance. Because numerical choices can have important effects (e.g., Tolman 1992; Hargreaves and Annan 2000), a few details should be given. All calculations are performed within the WAVEWATCH III modeling framework (Tolman 2008, 2009; hereinafter WWATCH), using the third-order spatial and spectral advection scheme, and including modifications of the source terms described here. The source terms are integrated with the fully implicit scheme of Hargreaves and Annan (2000), combined with the adaptation time step and limiter method of Tolman (2002a), in which a



minimum time step of 10 s is used, so that the limiter on wind-wave growth is almost never activated. The diagnostic tail, proportional to f^{-5} , is only imposed at a cutoff frequency f_c set to

$$f_c = f_{FM} f_m. \quad (7)$$

Here, we take $f_{FM} = 10$ and define the mean frequency as $f_m = 1/T_{m0,1}$. Hence, f_c is generally above the maximum model frequency that we fixed at 0.72 Hz, and the high-frequency tail is left to evolve freely. Some comparison tests are also performed with other parameterizations using a lower value of f_c , typically set at $2.5f_m$ (Bidlot et al. 2007a). In such calculations, although the net source term may be nonzero at frequencies above f_c , there is no spectral evolution due to the imposed tail.

a. Nonlinear wave–wave interactions

All the results discussed and presented in this section are obtained with the discrete interaction approximation (DIA) of Hasselmann et al. (1985). The coupling coefficient that gives the magnitude of the interactions is C_{nl} . Based on comparisons with exact calculations, Komen et al. (1984) adjusted the value of C_{nl} to 2.78×10^7 , which is the value used by Bidlot et al. (2005). Here, this constant will be modified slightly. The DIA parameterization is well known for its shortcomings (Banner and Young 1994), and the adjustment of other parameters probably compensates for some of these errors. This matter will be fully discussed in a future publication.

b. Swell dissipation

Observations of swell dissipation are consistent with the effects of friction at the air–sea interface (Ardhuin et al. 2009a), resulting in a flux of momentum from the wave field to the wind (Harris 1966). We thus write the swell dissipation as a negative contribution S_{out} , which is added to S_{in} to make the wind-wave source term S_{atm} .

Using the method of Collard et al. (2009), a systematic analysis of swell observations by Ardhuin et al. (2009a) showed that the swell dissipation is nonlinear, which is possibly related to a laminar-to-turbulent transition of the oscillatory boundary layer over swells. Defining the boundary Reynolds number $Re = 4u_{orb}a_{orb}/\nu_a$, where u_{orb} and a_{orb} are the significant surface orbital velocity and displacement amplitudes, and ν_a is the air viscosity, we take, for Re less than a critical value Re_c ,

$$S_{out}(k, \theta) = -C_{dsv} \frac{\rho_a}{\rho_w} (2k\sqrt{2\nu\sigma}) F(k, \theta), \quad (8)$$

where the constant C_{dsv} is equal to 1 in Dore (1978)'s laminar theory and the radian frequency σ is related to k via the dispersion relation.

When the boundary layer is expected to be turbulent, for $Re \geq Re_c$, we take

$$S_{out}(k, \theta) = -\frac{\rho_a}{\rho_w} (16f_e \sigma^2 u_{orb}/g) F(k, \theta). \quad (9)$$

A few tests have indicated that a threshold $Re_c = (2 \times 10^5 m)/H_s$ provides reasonable results, although it may also be a function of the wind speed, and we have no explanation for the dependence on H_s . A constant threshold close to 2×10^5 provides similar—but less accurate—results. Here, we shall use $C_{dsv} = 1.2$.

The parameterization of the turbulent boundary layer is a bit more problematic and, in the absence of direct measurements in the boundary layer, leaves room for speculations. Assuming a constant f_e in (9), Ardhuin et al. (2009b) found that swell observations are consistent with $0.004 < f_e < 0.013$. From the analogy with an oscillatory boundary layer over a fixed bottom (Jensen et al. 1989), these values correspond to a surface with a very small roughness. Because we also expect the wind to influence f_e , we include the adjustable effects of wind speed on the roughness, and an explicit correction of f_e in the form of a Taylor expansion to first order in u_*/u_{orb} :

$$f_e = s_1 \left\{ f_{e,GM} + [|s_3| + s_2 \cos(\theta - \theta_u)] \frac{u_*}{u_{orb}} \right\}, \quad (10)$$

where $f_{e,GM}$ is the friction factor given by Grant and Madsen's (1979) theory for rough oscillatory boundary layers without a mean flow. Adequate swell dissipation is obtained with constant values of f_e in the range 0.004–0.007, but these do not necessarily produce the best results when comparing wave heights to observations. Based on the simple idea that most of the air–sea momentum flux is supported by the pressure–slope correlations that give rise to the wave field (Donelan 1998; Peirson and Banner 2003), we have set the surface roughness seen by the oscillatory flow z'_0 to a small fraction of that seen by the mean flow z_0 :

$$z'_0 = r_{z0} z_0. \quad (11)$$

Here, r_{z0} is here set to 0.04. As a result, typical values of a_{orb}/z'_0 are as large as 2×10^5 , with $f_{e,GM}$ of the order of 0.003.

The coefficients s_2 and s_3 of the $O(u_*/u_{orb})$ correction have been adjusted to -0.018 and 0.015 , respectively, the former negative value giving a stronger dissipation for swells opposed to winds, when $\cos(\theta - \theta_u) < 0$. This gives a range of values of f_e consistent with the observations, and reasonable hindcasts of swell decay (Fig. 1), with a small underestimation of dissipation for steep

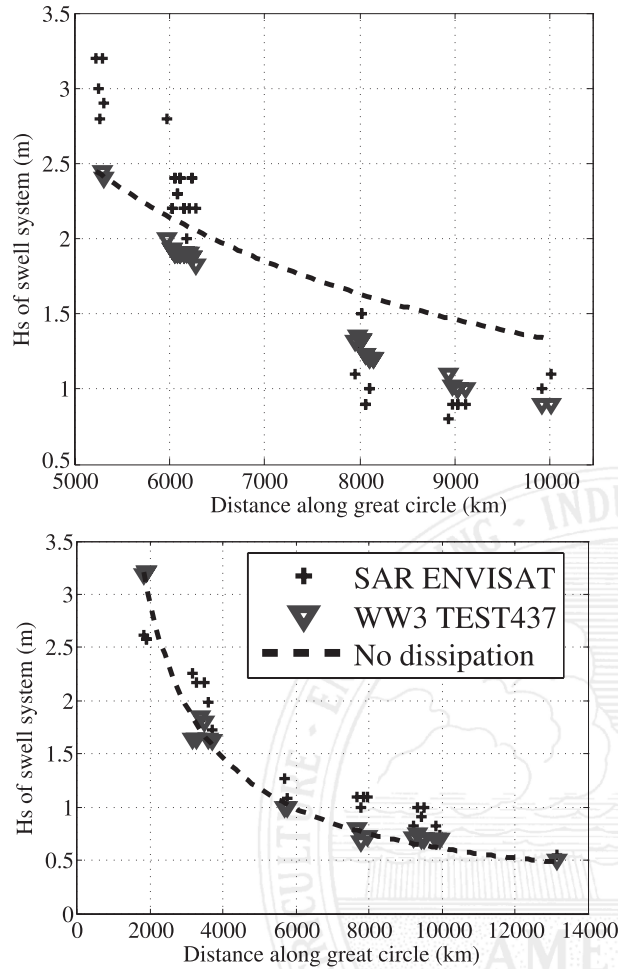


FIG. 1. Comparison of modeled swell significant heights, following the propagation of the two swells shown by Ardhuin et al. (2009) with peak periods of 15 s and (top) high or (bottom) low dissipation rates. Known biases in the level 2 data have been corrected following Collard et al. (2009).

AU14

swells. Because an increase of s_1 from 0.8 to 1.1 produces negative biases on H_s of the order of 30% at all oceanic buoys, the magnitude of the swell dissipation cannot be much larger than chosen here.

Further validation of the swell dissipation is provided by the global-scale hindcasts in section 4.

c. Wave breaking

Observations show that waves break when the orbital velocity at their crest, U_c , comes close to the phase speed, C , with a ratio $U_c/C > 0.8$ for random waves (Tulin and Landrini 2001; Stansell and MacFarlane 2002; Wu and Nepf 2002). It is nevertheless difficult to parameterize the breaking of random waves, since the only available wave information here are the spectral densities $F(k, \theta)$. These densities can be related to the

orbital velocity variance in a narrow frequency band. This question is addressed in detail by Filipot et al. (2010). Yet, a proper threshold has to be defined for this quantity, and the spectral rate of energy loss associated with breaking has to be defined. Also, breaking is intricately related to the complex nonlinear evolution of the waves (e.g., Banner and Peirson 2007).

These difficulties will be ignored here. We shall parameterize the spectral dissipation rate directly from the wave spectrum, in a way similar to WZB. Essentially, we distinguish between spontaneous and induced breaking, the latter being caused by large-scale breakers overtaking shorter waves, resulting in their dissipation. For the spontaneous breaking we parameterize the dissipation rate directly from the spectrum, without the intermediate step of estimating a breaking probability.

We started from the simplest possible dissipation term formulated in terms of the direction-integrated spectral saturation $B(k)$ given by Eq. (5), with a realistic threshold $B_{or} = 1.2 \times 10^{-3}$ corresponding to the onset of wave breaking (Babanin and Young 2005). This saturation parameter corresponds exactly to the α parameter defined by Phillips (1958). The value $B_0 = 8 \times 10^{-3}$, given by Phillips, corresponds to a self-similar sea state in which waves of all scales have the same shape, limited by the breaking limit.

This view of the sea state, however, ignores completely wave directionality. Early tests of parameterizations based on this definition of B indicated that the spectra were too narrow (Ardhuin and Le Boyer 2006). This effect could be due to many errors. Because Banner et al. (2002) introduced a directional width in their saturation to explain some of the variability in the observed breaking probabilities, we similarly modify the definition of B . Expecting also to have different dissipation rates in different directions, we define a saturation B' that would correspond, in deep water, to a normalized velocity variance projected in one direction (in the case $s_B = 2$), with a further restriction of the integration of directions controlled by Δ_θ :

$$B'(k, \theta) = \int_{\theta - \Delta_\theta}^{\theta + \Delta_\theta} k^3 \cos^{s_B}(\theta - \theta') F(k, \theta') \frac{C_g}{2\pi} d\theta'. \quad (12)$$

Here, we shall always use $\Delta_\theta = 80^\circ$. In our model, a sea state with two systems with the same energy but of opposite direction will thus produce less dissipation than a sea state with all the energy radiated in the same direction.

We finally define our dissipation term as the sum of the saturation-based term of Ardhuin et al. (2008a) and a cumulative breaking term $S_{bk,cu}$:

$$S_{oc}(k, \theta) = \sigma \frac{C_{ds}^{sat}}{B_r^2} \left\{ \begin{array}{l} \delta_d \max[B(k) - B_r, 0]^2 \\ + (1 - \delta_d) \max[B'(k, \theta) - B_r, 0]^2 \end{array} \right\} F(k, \theta) + S_{bk,cu}(k, \theta) + S_{turb}(k, \theta), \quad (13)$$

where

$$B(k) = \max\{B'(k, \theta), \theta \in [0, 2\pi]\}. \quad (14)$$

AU3 The combination of an isotropic part (the term that multiplies δ_d) and a direction-dependent part (the term with $1 - \delta_d$) was intended to allow some control of the directional spread in the resulting spectra. This aspect is **F2** illustrated in Fig. 2 with a hindcast of the 3 November 1999 case during the Shoaling Waves Experiment (SHOWEX; Ardhuin et al. 2007). Clearly, the isotropic saturation in the TEST442 dissipation (with the original threshold $B_r = 0.0012$) produces very narrow spectra, even though it is known that the DIA parameterization for nonlinear interactions tends to broaden the spectra. The same pattern of behavior is obtained with the isotropic parameterization by van der Westhuysen et al. (2007), as demonstrated by Ardhuin and Le Boyer (2006). Further, using an isotropic dissipation at all frequencies yields an energy spectrum that decays faster toward high frequencies than the observed spectrum (Fig. 2a). On the contrary, a fully directional dissipation term (TEST443 with $\delta_d = 0$) gives a better fit for all of the parameters. With $s_B = 2$, we reduce B_r to 0.0009, a threshold for the onset of breaking that is consistent with the observations of Banner et al. (2000) and Banner et al. (2002), as discussed by Babanin and van der Westhuysen (2008). The overall dissipation term in TEST443 is anisotropic due to the cumulative effect, but this does not significantly alter the underestimation of the directional spread.

The dissipation constant C_{ds}^{sat} was adjusted to 2.2×10^{-4} in order to give acceptable time-limited wave growth and good directional fetch-limited growth as described by Ardhuin et al. (2007). As noted in this previous work, similar growth patterns in wave energy with fetch are possible with almost any magnitude of the wind input, but a reasonable mean direction in slanting fetch conditions selects the range of possible levels of input. Here, the mean directions at the observed peak frequency are still biased by about 25° toward the alongshore direction with the parameterizations proposed here (Fig. 2b), which is still less than the 50° obtained with the weaker Tolman and Chalikov (1996) source terms (Ardhuin et al. 2007, Fig. 11). A relatively better fit is obtained with the BAJ parameterization. This is likely due to either the stronger wind input or the weaker dissipation at the peak. ~~It is likely that both features of the BAJ parameterization are more realistic than what we propose here.~~

The equilibrium sea state, achieved by most models for long durations with steady wind and infinite fetch, and often compared with the Pierson and Moskowitz (1964) spectrum, is largely controlled by the balance between the nonlinear flux of energy to low frequencies and the wind output term, as discussed below. Figure 3 shows the fetch-limited growth in wave energy of the various parameterizations. We repeat here the sensitivity test to the presence of swell, ~~which has already been~~ displayed in Ardhuin et al. (2007). Whereas the 1-m swell causes an unrealistic doubling of the wind sea energy at short fetch in the BAJ parameterization, the new parameterizations, just like the one by van der Westhuysen et al. (2007), are by design insensitive to swell (not shown). **F3**

The dissipation S_{turb} due to wave-turbulence interactions is expected to be much weaker (Ardhuin and Jenkins 2006) and will be neglected here.

Finally, following the analysis by Filipot et al. (2010), the threshold B_r is corrected for shallow water, so that B'/B_r in different water depths corresponds to the same ratio of the root-mean-square orbital velocity and phase speed. For periodic and irrotational waves, the orbital velocity increases much more rapidly than the wave height as it approaches the breaking limit. Further, due to nonlinear distortions in the wave profile in shallow water, the height can be twice as large as the height of linear waves with the same energy. To express a relevant threshold from the elevation variance, we consider the slope $kH_{lin}(kD)$ of an hypothetical linear wave that has the same energy as the wave of maximum height. In deep water,² $kH_{lin}(\infty) \approx 0.77$, and for other water depths we thus correct B_r by a factor $[kH_{lin}(kD)/kH_{lin}(\infty)]^2$. Using streamfunction theory (Dalrymple 1974), a polynomial fit as a function of $Y = \tanh(kD)$ gives

$$B'_r = B_r Y (M_4 Y^3 + M_3 Y^2 + M_2 Y + M_1), \quad (15)$$

such that $B'_r = B_r$ in deep water. The fitted constants are $M_4 = 1.3286$, $M_3 = -2.5709$, $M_2 = 1.9995$, and $M_1 = 0.2428$. Although this behavior is consistent with the variation of the depth-limited breaking parameter γ derived empirically by Ruessink et al. (2003), the resulting dissipation rate is not yet expected to produce realistic results

² This value of the maximum equivalent linear height, $H_{lin} = 2\sqrt{2E}$, with E being the elevation variance, is smaller than the usual value $kH = 0.88$ due to the correction for the nonlinear wave profile for which $H > \sqrt{2E}$.

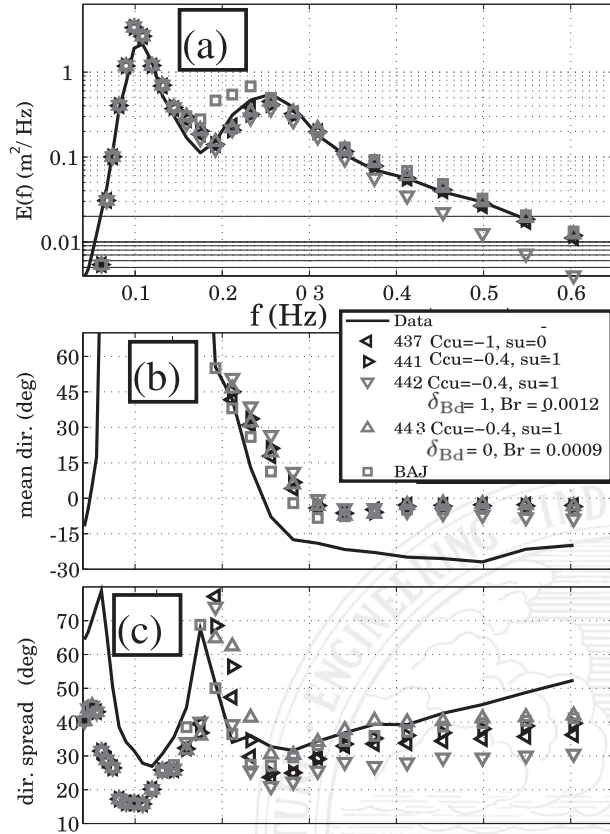


FIG. 2. Wave spectra on 3 Nov 1999 at buoy X3 (fetch, 39 km; wind speed $U_{10} = 9.4 \text{ m s}^{-1}$), averaged over the time window 1200–1700 EST, from observations and model runs, with different model parameterizations (symbols): BAJ stands for Bidlot et al. (2005). The (a) energy, (b) mean direction, and (c) directional spread are shown. This figure is analogous to Figs. 10 and 11 in Ardhuin et al. (2007), and the model forcing and setting are identical. It was further verified that halving the resolution from 1 km to 500 m does not affect the results. All parameterizations settings are listed in Tables A1 and A2. Input parameters for TEST443 are identical to those for TEST441, and TEST442 differs from TEST441 only in its isotropic direct breaking term, given by $s_B = 0$, $\Delta_\theta = 180^\circ$, and $B_r = 0.0012$.

for surf zones because no effort was made to verify this aspect. This is the topic of ongoing work, which is outside of the scope of the present paper.

The cumulative breaking term $S_{\text{bk,cu}}$ represents the smoothing of the surface by big breakers with celerity C' that wipe out smaller waves of phase speed C . Due to uncertainties in the estimation of this effect in the observations of Young and Babanin (2006), we use the theoretical model of Ardhuin et al. (2009b). Briefly, the relative velocity of the crests is the norm of the vector difference, $\Delta_c = |\mathbf{C} - \mathbf{C}'|$, and the dissipation rate of short wave is simply the rate of passage of the large breaker over short waves, that is, the integral of $\Delta_c \Lambda(\mathbf{C}) d\mathbf{C}$, where $\Lambda(\mathbf{C}) d\mathbf{C}$ is the length of breaking crests per unit surface that has velocity components between C_x and $C_x + dC_x$, and

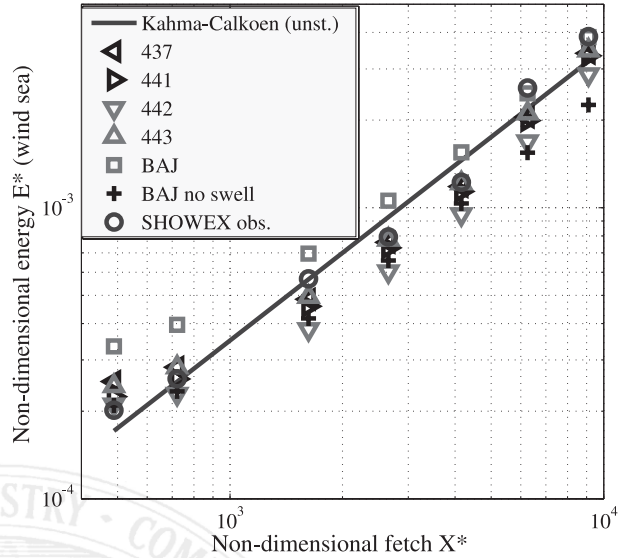


FIG. 3. Fetch-limited growth of the windsea energy as a function of fetch on 3 Nov 1999, averaged over the time window 1200–1700 EST, from observations and model runs, with different model parameterizations (symbols): BAJ stands for Bidlot et al. (2005). This figure is analogous to Fig. 8 in Ardhuin et al. (2007), the model forcing and settings are identical. All parameters for BAJ, TEST441, and TEST443 are listed in Tables A1 and A2. The input parameters for TEST443 are identical to those for TEST441, and TEST442 differs from TEST441 only in its isotropic direct breaking term, given by $s_B = 0$, $\Delta_\theta = 180^\circ$, and $B_r = 0.0012$.

between C_y and $C_y + dC_y$ (Phillips 1985). Because there is no consensus on the form of Λ (Gemrich et al. 2008), we prefer to link Λ to the breaking probabilities. Based on Banner et al. [(2000, Fig. 6); $b_T = 22(\epsilon - 0.055)^2$], and taking their saturation parameter ϵ to be of the order of $1.6\sqrt{B'(k, \theta)}$, the breaking probability of dominant waves is approximately

$$P = 56.8[\max(\sqrt{B'(k, \theta)} - \sqrt{B'_r}, 0)]^2. \quad (16)$$

However, because they used a zero-crossing analysis for a given wave scale, there are many times when waves are not counted since the record is dominated by another scale: in their analysis there is only one wave at any given time. This tends to overestimate the breaking probability by a factor of 1.5–2 (Manasseh et al. 2006), compared to the present approach in which we consider that several waves (of different scales) may be present at the same place and time. We shall thus correct for this effect, by simply dividing P by 2.

With this approach we define the spectral density of the crest length (breaking or not) per unit surface $l(\mathbf{k})$ such that $\int l(\mathbf{k}) dk_x dk_y$ is the total length of all crests per unit surface, with a crest being defined as a local maximum of the elevation in one horizontal direction. In the wave-number vector spectral space we take

$$l(\mathbf{k}) = 1/(2\pi^2 k), \quad (17)$$

which is equivalent to a constant in wavenumber-direction space $l(k, \theta) = 1/(2\pi^2)$. This number was obtained by considering an ocean surface full of unidirectional waves, with one crest for each wavelength $2\pi/k$ for each spectral interval $\Delta k = k$; for example, one crest corresponding to spectral components in the range $0.5-1.5 k$. This potential number of crests is doubled by the directionality of the sea state. These two assumptions have not been verified and thus the resulting value of $l(\mathbf{k})$ is merely an adjustable order of magnitude.

Thus, the spectral density of the breaking crest length per unit surface is $\Lambda(\mathbf{k}) = l(\mathbf{k})P(\mathbf{k})$. Assuming that any

breaking wave instantly dissipates all the energy of all of the waves with frequencies higher by a factor r_{cu} or more, then the cumulative dissipation rate is simply given by the rate at which these shorter waves are taken over by larger breaking waves times the spectral density; namely,

$$S_{bk,cu}(k, \theta) = C_{cu} F(k, \theta) \int_{f' < r_{cu} f} \Delta_C \Lambda(\mathbf{k}') d\mathbf{k}', \quad (18)$$

where r_{cu} defines the maximum ratio of the frequencies of long waves that will wipe out the short waves.

We now obtain Λ by extrapolating Eq. (16) to higher frequencies. With $56.8/(4\pi^2) = 1.44$, it gives the source term

$$S_{bk,cu}(k, \theta) = -1.44 C_{cu} F(k, \theta) \int_0^{r_{cu} f} \int_0^{2\pi} \max(\sqrt{B(k', \theta')} - \sqrt{B_r}, 0)^2 \Delta_C d\theta' dk',$$

We shall take $r_{cu} = 0.5$, and C_{cu} is a tuning coefficient expected to be a negative number of order 1, which also corrects for errors in the estimation of l .

This generic form of the source terms produces markedly different balances for both mature and fully developed seas.

F4 For mature seas, without cumulative effect, Fig. 4 shows that a balance is possible that gives roughly the same energy level and wind input term up of to 0.4 Hz as the BAJ parameterization. However, the balance in the tail results in the energy level decreasing slower than f^{-4} as the dissipation is too weak compared to the input, and thus the nonlinear energy flux is reversed, pumping energy from the tail to lower frequencies.

The introduction of a strong cumulative term (TEST437) allows a balance at roughly the same energy level. However, with the present formulation this will lead to a dissipation that is too strong at high frequency for higher winds. The introduction of the sheltering effect via the parameter s_u (details in section 2d) is designed to reach a balance with a weaker cumulative effect.

The most important qualitative feature is the lack of a regular predefined shape for the normalized dissipation term, $S_{oc}(k, \theta)/E(k, \theta)$. Whereas the shape given by $\delta k + (1 - \delta)k^2$ is clearly visible in BAJ (with extremely high dissipation rates if one considers high frequencies), and the low- to high-frequency dissipation transition at $2f_p$ is evident in TC, the shapes of the new dissipation rates are completely dictated by the local spectral saturation level. This leads to a relatively narrow peak of dissipation right above the spectral peak, where the saturation is strongest.

This feature helps to produce realistic spectral shapes near the peak, with a steeper low-frequency side and a more gentle slope on the high-frequency side, contrary to the backward-facing spectra produced by BAJ and TC. However, this localized strong relative dissipation, $S_{oc}(k, \theta)/F(k, \theta)$, is hard to reconcile with the time and spatial scales of breaking events, and is thus probably exaggerated. Indeed, there should be no significant difference in the relative dissipation among the spectral components that contribute to a breaking wave crest, provided that they do not disperse significantly over the breaker lifetime, which is less than a wave period. There is no physical reason why a breaking event would take much more energy, relatively speaking, from the spectral band $(1.1-1.2)f_p$ than from $(1.2-1.3)f_p$. The factor of 2 difference found here in the relative dissipation rates thus appears to be unrealistic. This strong relative dissipation at the peak (50% higher than in BAJ) is one important factor that leads to slower growth of the wave spectrum in TEST441 compared to BAJ. It is possible that the localization of S_{oc} at the peak compensates for the broader spectrum produced by the DIA compared to results with an exact nonlinear interaction calculation.

We now consider “fully developed” conditions, as illustrated by Fig. 5. At low frequency, the nonlinear swell damping term S_{out} (the negative part of S_{in}) cancels about 30%–50% of the nonlinear energy flux, so that the sea state grows only very slowly. As a result, “full development” does not exist, but the resulting energy is still compatible with the observations of mature sea states (Alves et al. 2003). In contrast, the linear swell damping adjusted by Tolman (2002b) is designed to produce reasonable swell heights in the tropics, but it is much smaller

F5

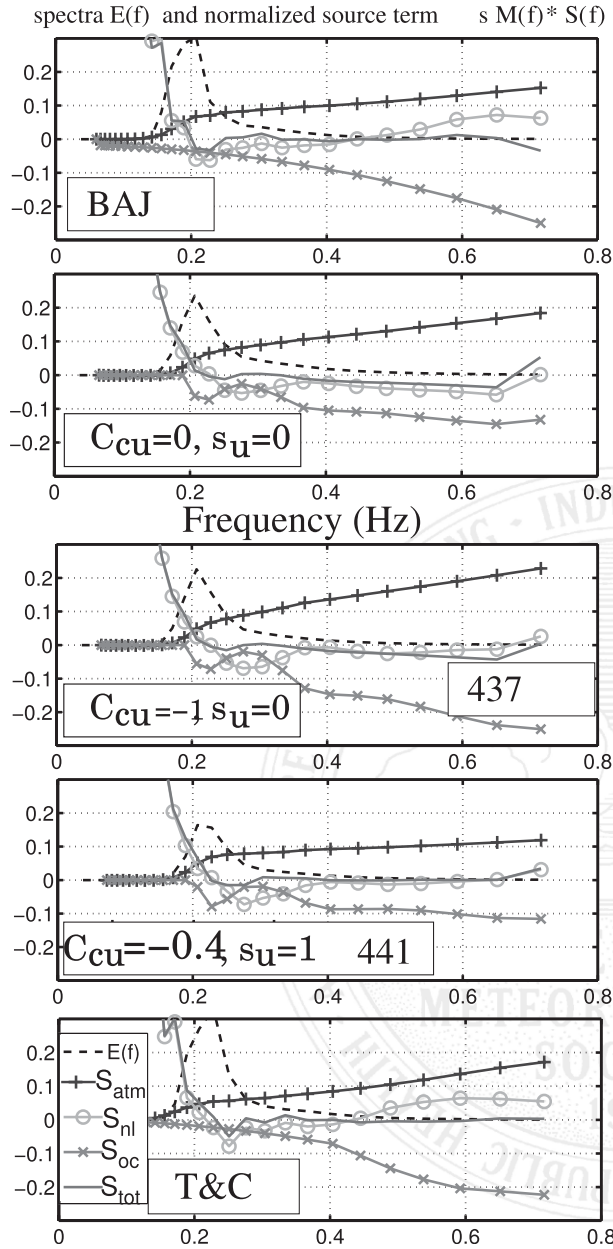


FIG. 4. Academic test case over a uniform ocean with a uniform 10 m s^{-1} wind starting from rest, after 8 h of integration, when $C_p/U_{10} \approx 1$. Source term balances are given by the parameterization BAJ, and the parameterizations proposed here with the successive introduction of the cumulative breaking and the wind-sheltering effects with the parameters C_{cu} and s_u . For BAJ, a diagnostic f^{-5} tail is applied above $2.5 \times$ the mean frequency. The source terms are multiplied by the normalization function $M(f) = \rho_w C / [\rho_a E(f) \sigma U_{10}]$. The TC stands for of Tolman and Chalikov (1996).

than the nonlinear energy flux to low frequencies, even with the reduced interaction coefficient proposed by Tolman and Chalikov (1996). A nonlinear swell dissipation appears to be necessary to obtain both a realistic

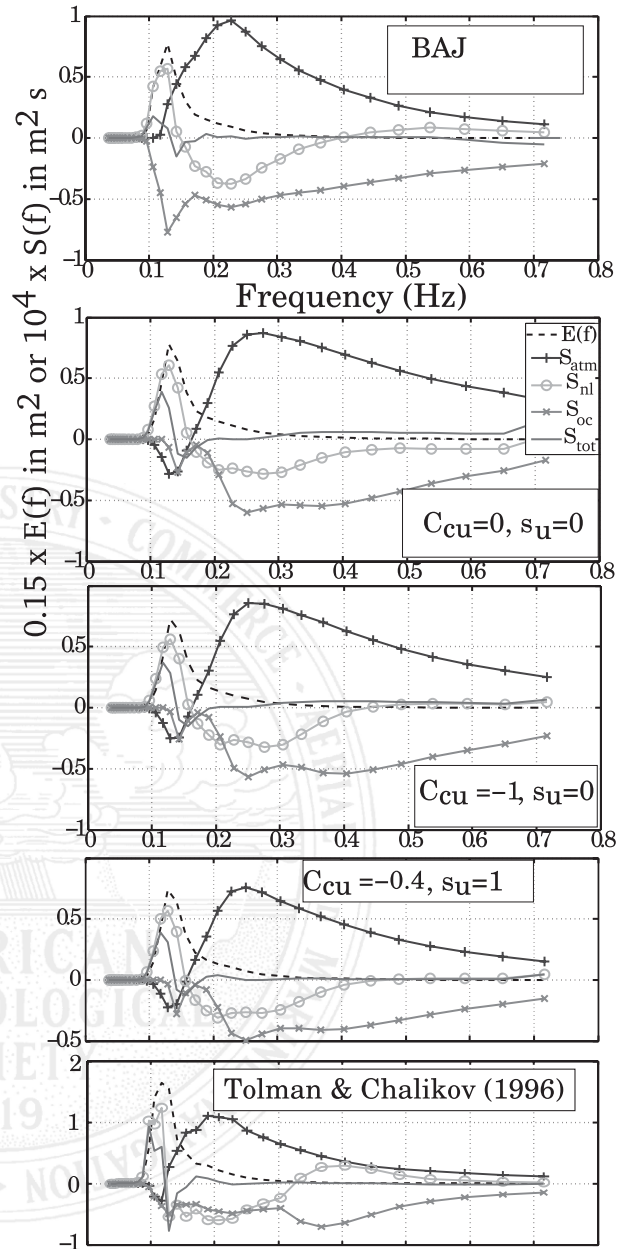


FIG. 5. As in Fig. 4, but after 48 h of integration and without normalization of the source terms. Source term balances are given by the parameterization BAJ, and the parameterizations proposed here with the successive introduction of the cumulative breaking and the wind-sheltering effects with the parameters C_{cu} and s_u .

damping of observed swells and a satisfactory agreement with mature wind waves. Nonlinearity also brings within the same order of magnitude the decay scales estimated for short (Högström et al. 2009) and very long swells (Ardhuin et al. 2009b).

Both parameterizations are physically very different from the parameterizations of the Komen et al. (1984) family, including Bidlot et al. (2005). In these cases, the

swell energy is lost to the ocean via whitecapping. Here, we propose that this energy is lost to the atmosphere, with an associated momentum flux that drives the wave-driven wind observed in wave flumes (Harris 1966) and for very weak winds at sea (Smedman et al. 2009).

In the inertial range, a reasonable balance of all the source terms is obtained for $C_{cu} = -0.4$ (Fig. 5). In this case, the spectrum approaches an f^{-4} shape up to 0.4 Hz. The behavior of the high-frequency tail is best seen when displayed in nondimensional form, as is done in Fig. 6. Figure 6 shows the unrealistically high level of the tail without cumulative effect nor modification of the wind input, and the equally unrealistic low tail with the BAJ parameterization, especially when the tail is left to evolve freely. With the TEST441 parameterization ($C_{cu} = 0.4$ and $s_u = 1$), the spectral level at 0.7 Hz (3 m wavelength) may be 30% too high compared to other analyses by Long and Resio (2007), but the resulting spectral moments m_3 is still slightly underpredicted (Ardhuin et al. 2009b). Spectral levels for shorter waves (20 cm–2 m) were estimated at $\alpha = 1.8 \times 10^{-3}$ by Banner et al. (1989). There is thus a strong need for more spectral measurements in the range of wavelengths from 0.5 to 5 m, outside of the range of buoy measurements.

Adding the cumulative effect can be a means of controlling the tail level, but this degree of freedom is not enough. Indeed, in strongly forced conditions the dominant waves break frequently, and a high cumulative effect, $C_{cu} = -1$, reduces the energy level in the tail below observed levels. This effect can be verified with mean square slopes estimated from satellite altimeter measurements (Fig. 8), or high moments of the frequency spectrum derived from buoy data (not shown but similar).

A more accurate shape of the spectrum tail may be obtained with a lower C_{cu} or a higher r_{cu} , so that dominant breaking waves will only wipe out much smaller waves. Instead, and because the wind to wave momentum flux was too high in high winds, we chose to introduce one more degree of freedom, allowing a reduction of the wind input at high frequency.

d. Wind input

The wind input parameterization is thus adapted from Janssen (1991; see also Chalikov 1991) and the following adjustments performed by Bidlot et al. (2005, 2007a). The full wind input source term reads

$$S_{in}(k, \theta) = \frac{\rho_a \beta_{max}}{\rho_w \kappa^2} e^{Z} Z^4 \left(\frac{u_*^2}{C} \right) \times \max[\cos(\theta - \theta_u), 0]^p \sigma F(k, \theta), \quad (19)$$

where β_{max} is a nondimensional growth parameter (constant) and κ is von Kármán's constant. In the present

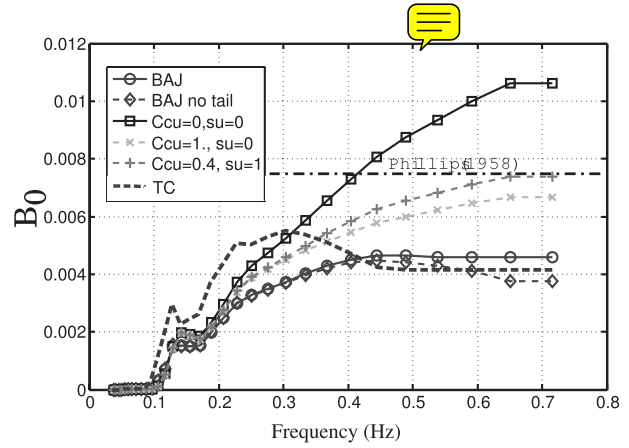


FIG. 6. Values of the spectral saturation B_0 for the cases presented in Fig. 5.

implementation the air–water density ratio is constant. The power of the cosine is taken constant with $p = 2$. We define the effective wave age $Z = \log(\mu)$, where μ is given by Janssen (1991; see also Chalikov 1991), and corrected for intermediate water depths, so that

$$Z = \log(kz_1) + \kappa / [\cos(\theta - \theta_u)(u_* / C + z_\alpha)], \quad (20)$$

where z_1 is a roughness length modified by the wave-supported stress τ_w and z_α is a wave age tuning parameter. We define z_1 implicitly by

$$U_{10} = \frac{u_*}{\kappa} \log\left(\frac{z_u}{z_1}\right), \quad (21)$$

$$z_0 = \min\left(\alpha_0 \frac{\tau}{g}, z_{0,max}\right), \quad \text{and} \quad (22)$$

$$z_1 = \frac{z_0}{\sqrt{1 - \tau_w / \tau}}, \quad (23)$$

where z_u is the height at which the wind speed is specified, usually 10 m. The maximum value of z_0 was added to reduce possible unrealistic wind stresses at high winds that are otherwise given by the standard parameterization. For example, $z_{0,max} = 0.0015$ is equivalent to setting a maximum wind drag coefficient of 2.5×10^{-3} . For the TEST441 parameterization, we have adjusted $z_\alpha = 0.006$ and $\beta_{max} = 1.52$ (Fig. 7).

An important part of the parameterization is the calculation of the wave-supported stress τ_w , which includes the resolved part of the spectrum, as well as the growth of an assumed f^{-5} diagnostic tail beyond the highest frequency. This parameterization is highly sensitive to the high-frequency part of the spectrum since a high energy level there will lead to a larger value of z_1 and u_* , which gives a positive feedback and reinforces the energy levels.

F6

AU4

F7

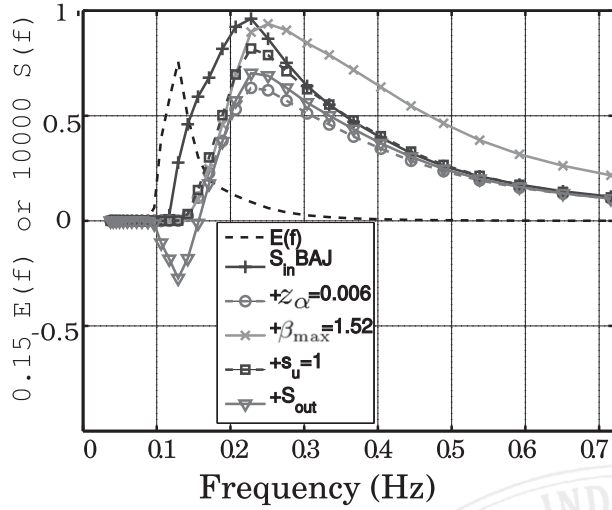


FIG. 7. Incremental adjustments to the wind-wave interaction source term S_{atm} , going from the BAJ form to the one used in TEST441. From one curve to the next, only one parameter is changed. Different S_{atm} are given for the same wave spectrum, previously obtained by running the model from a calm sea for 8 h with the BAJ parameterization and a wind speed of 10 m s^{-1} .

To allow a balance with the saturation-based dissipation, the wind input at high frequency is reduced by modifying the friction velocity u_* . This correction also reduces the drag coefficient at high winds. In particular, the wind input is reduced for high frequencies and high winds, loosely following Chen and Belcher (2000). This is performed by replacing u_* in Eq. (19) with a wave-number-dependent $u'_*(k)$ defined by

$$(u'_*)^2 = u_*^2 (\cos\theta_u, \sin\theta_u) - |s_u| \int_0^k \int_0^{2\pi} \frac{S_{\text{in}}(k', \theta)}{C} (\cos\theta, \sin\theta) dk' d\theta, \quad (24)$$

where the sheltering coefficient $|s_u| \sim 1$ can be used to tune the wind stresses for high winds, which would be largely overestimated for $s_u = 0$. For $s_u > 0$, this sheltering is also applied within the diagnostic tail, which requires the estimation of a three-dimensional lookup table for the high-frequency stress. The shape of the new wind input is illustrated in Fig. 7 for fully developed seas. Clearly, for relatively young waves the energy levels at the spectral peak are lower with $s_u = 1$ (TEST441) than in other runs; this is largely due to a reduced feedback of the wave age on the wind stress via the τ_w/τ term in Eq. (23). The reduction of z_α from 0.011 to 0.006 strongly reduces the input for frequencies in the range 0.15–0.2 Hz, which is probably overestimated in BAJ when average (20%) levels of gustiness are considered: now the wind input goes to zero for $f = 0.13$, which corresponds to $C/U_{10} = 0.83$, whereas it is still significant at

that wave age in the BAJ parameterization. As a result the much lower input level needs a readjustment, performed here by increasing β_{max} to 1.52. Yet, this high value of β_{max} produces very high wind stress values and thus a very strong high-frequency input. Adding the sheltering term $s_u = 1$ allows a decent balance at high frequency. Finally, the addition of the air-sea friction term that gives swell dissipation produces a significant reduction of the input to the wind sea at $f = 0.25$ Hz. It is questionable whether this mechanism also applies in the presence of the critical layer for those waves. This matter clearly requires more theoretical and experimental investigation.

3. Consequences of the source term shape

We have already illustrated the effects of various parameters on spectral shapes in academic time-limited and more realistic fetch-limited conditions. We now look at real sea states observed in the World Ocean. Although wave spectra are difficult to compare to the few available observations, we have investigated the systematic variation of spectral moments:

$$m_n(f_c) = \int_0^{f_c} \int_0^{2\pi} f^n F(f, \theta) d\theta df, \quad (25)$$

with $n = 2, 3$, and 4, and cutoff frequencies in the range 0.2–0.4 Hz. The spectral density $F(f, \theta)$ is estimated as $2\pi F(k, \theta)/C_g$, using linear wave theory. Such moments are relevant to a variety of applications. Ardhuin et al. (2009b) investigated the third moment, which is proportional to the surface Stokes drift in deep water, and found that buoy data are very well represented by a simple function of U_{10} , H_s , and f_c , which typically explains 95% of the variance of m_3 .

This relationship is well reproduced in hindcasts using $C_{\text{cu}} = -0.4$ and $s_u = 1$, while the BAJ source terms give almost a constant value of m_3 when H_s varies and U_{10} is fixed (Ardhuin et al. 2009b).

Here, we consider the fourth moment m_4 , which, for linear waves, is proportional to a surface mean square slope filtered at the frequency f_c . For modeled values a constant 0.011 is added to account for the short waves that contribute to the satellite signal and that are not resolved in the model. This saturated high-frequency tail, independent of wind speed, is consistent with the observations of Banner et al. (1989) and Vandemark et al. (2004).

Figure 8 shows that for any given wind speed m_{3c} increases with the wave height (Gourrion et al. 2002), whereas this is not the case for m_4 in the BAJ parameterization, or, for very high winds, when C_{cu} is too strong. In the case of BAJ, this is due to the $(k/k_r)^2$ part in the

[F8]

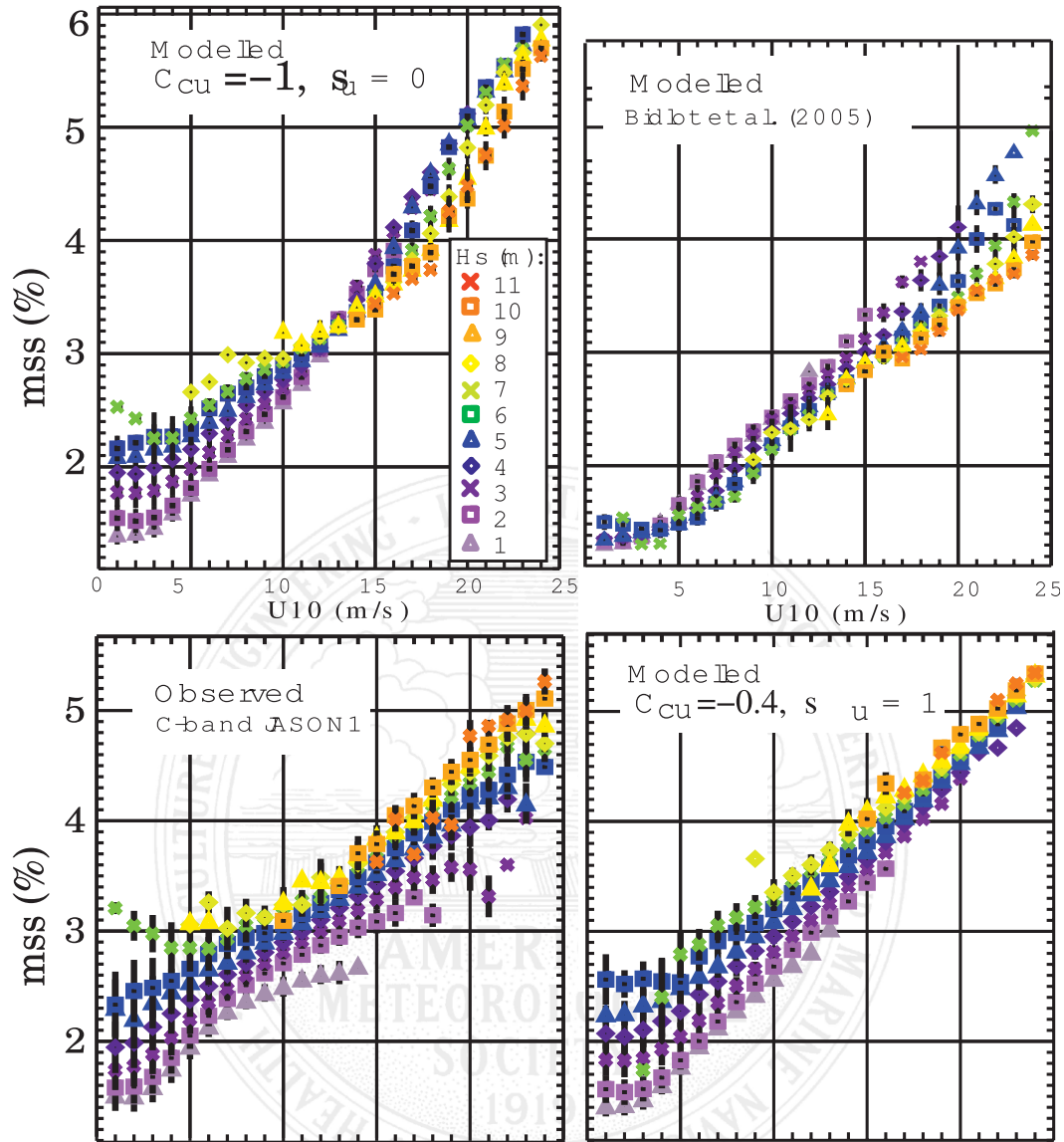


FIG. 8. Variation of the surface mean square slope estimated as either (bottom left) $0.64/\sigma_0$ using the C-band altimeter on board *Jason-1* after the correction of a 1.2 dB bias in the Jason data; or by integration of modeled spectra from 0 to 0.72 Hz, with either (bottom right) the $C_{cu} = -0.4$ and $s_u = 1$ parameterization (TEST441) or the (top right) parameterization by BAJ. The original 1-Hz data from Jason is subsampled at 0.5 Hz and averaged over 10 s (i.e., 58 km along the satellite track). The same averaging is applied to the wave model result, giving the total of 393 382 observations reported here, for the first half-year of 2007.

AU15

dissipation term [Eq. (2)], which plays a role similar to the cumulative term in our formulation. For $C_{cu} = -1$ and $s_u = 0$, the cumulative effect gets too strong for wind speeds over 10 m s^{-1} , in which case m_4 starts to decrease with increasing wave height, whereas for high winds and low (i.e., young) waves, the high-frequency tail is too high and the mean square slope gets to be as large as 6%, which is unrealistic. For $s_u = 0$ the high-frequency tail responds too much to the wind, hence our use of $s_u = 1$ in the TEST441 combination. The presence of a cumulative

dissipation term allows for a different balance in the spectral regions above the peak, where an equilibrium range with a spectrum proportional to f^{-4} develops (Long and Resio 2007), and in the high-frequency tail where the spectrum decays like f^{-5} or possibly a little faster. The spectral level in the range 0.2–0.4 Hz was carefully compared against buoy data and was found to be realistic.

These interpretations rely on the assumption that the model results are really wavenumber spectrum $E(\theta)$ converted to frequency densities using linear wave theory,

which is expected to be closer to the frequency spectra obtained from Lagrangian buoy measurements, and the wavenumber spectrum of nonlinear waves (Janssen 2009). This matter is left for further studies, together with a detailed interpretation of the altimeter radar cross sections. Although it covers much less data, the analysis of m_4 obtained from buoy heave spectra produces results similar to Fig. 8.

4. Verification

To provide simplified measures of the difference between the model time series X_{mod} and the observations X_{obs} , we use the following definitions for the normalized root-mean-square error (NRMSE),

$$\text{NRMSE}(X) = \sqrt{\frac{\sum (X_{\text{obs}} - X_{\text{mod}})^2}{\sum X_{\text{obs}}^2}}; \quad (26)$$

the normalized bias,

$$\text{NB}(X) = \sqrt{\frac{\sum X_{\text{obs}} - X_{\text{mod}}}{\sum X_{\text{obs}}}}; \quad \text{and} \quad (27)$$

Pearson's linear correlation coefficient,

$$r(X) = \frac{\sum (X_{\text{obs}} - \overline{X_{\text{obs}}})(X_{\text{mod}} - \overline{X_{\text{mod}}})}{\sqrt{\sum (X_{\text{obs}} - \overline{X_{\text{obs}}})^2 \sum (X_{\text{mod}} - \overline{X_{\text{mod}}})^2}}, \quad (28)$$

where the overbar denotes the arithmetic average.

The normalization of the errors allows a quantitative comparison between widely different sea state regimes. Because previous studies have often used (nonnormalized) RMSEs, we also provide RMSE values. In addition to the coastal fetch-limited case of SHOWEX, presented above, the parameterizations are calibrated on at the global scale and validated in two other cases.

a. Global-scale results

We present here results for the entire year 2007, using a stand-alone 0.5° resolution grid, covering the globe from 80° south to 80° north. The model has actually been adjusted to perform well over this dataset, but the very large number of observations (over 2 million altimeter collocation points) makes the model robust and an independent validation on 2008 gives identical results. The interested reader may also look at the monthly reports for the Service Hydrographique et Océanographique de la Marine (SHOM) model (e.g., Bidlot 2008), generated

as part of the model verification project of the Intergovernmental Oceanographic Commission–World Meteorological Organization (IOC–WMO) Joint Commission on Oceanography and marine Meteorology (JCOMM), in which the TEST441 parameterization ($C_{\text{cu}} = -0.4$ and $s_u = 1$) is used, except for the Mediterranean where, the TEST405 has been preferred for its superior performance for younger seas. These SHOM models are run in a combination of two-way nested grids (Tolman 2007). The monthly JCOMM reports include both analyses and forecasts, and many SHOM forecasts from December 2008 to June 2009 have been affected by wind file transfer problems.

Comparing the model results for H_s to well-calibrated altimeter-derived measurements (Queffelec and Croizé-Fillon 2008) provides a good method of verification for the model performance in a number of different wave climates. Figure 9 shows that, as expected, the important positive bias in the swell-dominated regions when using the BAJ parameterization has been largely removed. This is essentially the signature of the specific swell dissipation that is parameterized in S_{out} . The largest bias pattern now appears in the Southern Ocean, reaching 30 cm in the southern Atlantic. Although this bias is small compared to the local averaged wave height, it is rather odd when the model errors are plotted as a function of wave height in Fig. 10. Why would the model overestimate the Southern Ocean waves but underestimate the very large waves?

The structure of the large bias, also seen in model results of BAJ, is reminiscent of the observed pattern in iceberg distribution noticed by Tournadre et al. (2008). Assuming a full blocking of wave energy by icebergs larger than 1 km in diameter is enough to cancel most of the bias. ~~These observed iceberg distributions are enough to give a cross section for incoming waves of the order of 1%–10% for a 250-km propagation length. Taking icebergs into account could actually reverse the sign of the bias. This matter will be investigated elsewhere.~~

Also noticeable is a significant negative bias in the equatorial South Pacific, amplified from the same bias obtained with the BAJ parameterization. It is possible that the masking of subgrid islands (Tolman 2003) introduces a bias by neglecting shoreline reflections. This model defect could be exacerbated in this region by the very large ratio of shoreline length to sea area. This will also require further investigation. Finally, the negative biases for H_s along midlatitude east coasts are reduced but still persist. It is well known that these areas are also characterized by strong boundary currents (such as the Gulf Stream, Kuroshio, and Agulhas current) with warm waters that are generally conducive to wave amplification and faster wind-wave growth (e.g., Vandemark et al.

F9

F10

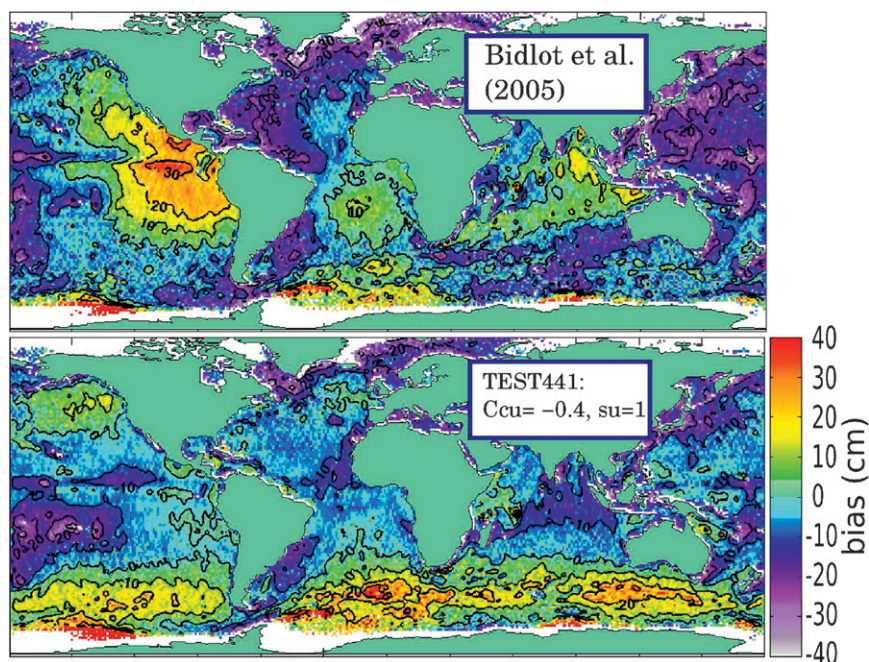


FIG. 9. The bias (cm) for the year 2007. The global 0.5 WWATCH model is compared to altimeters aboard the *Jason-1*, the *Environmental Satellite (Envisat)*, and *Geosat Follow-On (GFO)* satellite following the method of Raschle et al. (2008). (top) The result with the BAJ parameterization, and (bottom) the result with the $C_{cu} = -0.4$ and $s_u = 1$ (TEST441) parameterization.

2001). Neither effect is included in the present calculation because the accuracy of both modeled surface currents and air-sea stability parameterizations are likely to be insufficient (Collard et al. 2008; Ardhuin et al. 2007).

The reduction of systematic biases clearly contributes to the reduction of RMSEs, as is evident in the equatorial eastern Pacific (Fig. 11). However, the new parameterization also brings a considerable reduction to the scatter, with reduced errors even where biases are minimal, such as the trade winds area south of Hawaii, where the NRMSE for H_s can be as low as 5%. When areas within 400 km from continents are excluded, because the global model resolution may be inadequate, significant errors (>12.5%, in yellow to red) remain in the northern Indian Ocean, on the North American and Asian east coasts, and in the southern Atlantic. The parameterizations TEST405, TEST437, and TEST441 produce smaller errors on average than BAJ. It is likely that the model benefits from the absence of swell influences on wind seas: swell in BAJ typically leads to a reduced dissipation and stronger wind wave growth. As models are adjusted to average sea state conditions, this adjustment leads to reduced wind sea growth along east coasts, where there is generally less swell.

For the highest waves, the model scatter is smallest, with some important biases for some parameterizations.

Although the altimeter estimates are not expected to be valid for H_s larger than about 12 m, due to the low backscatter and a waveform that is too short to properly estimate H_s , this good model performance contradicts some claims (e.g., Cavaleri 2009) that models may be more inaccurate for severe weather.

Although much more sparse than the altimeter data, the in situ measurements collected and exchanged as part as the JCOMM wave model verification are very useful for constraining other aspects of the sea state. This is illustrated here with mean periods T_{m02} for data provided by the U.K. and French meteorological services, and peak periods T_p for all other sources. It is worth noting that the errors in H_s for in situ platforms are comparable to the errors found for altimeter data.

With the BAJ parameterizations, the largest errors in the model results are the 1.2–1.8 s biases in peak periods along the U.S. west coast (Fig. 12), and the underestimation of peak periods along the U.S. east coast. However, peak and mean periods off the European coasts are generally very well predicted. When using the TEST441 parameterization, the explicit swell dissipation reduces the bias over periods along the U.S. west coast, but the problem is not completely solved, with residual biases of 0.2–0.4 s. This is consistent with the validation using satellite synthetic aperture radar (SAR)

F11

F12

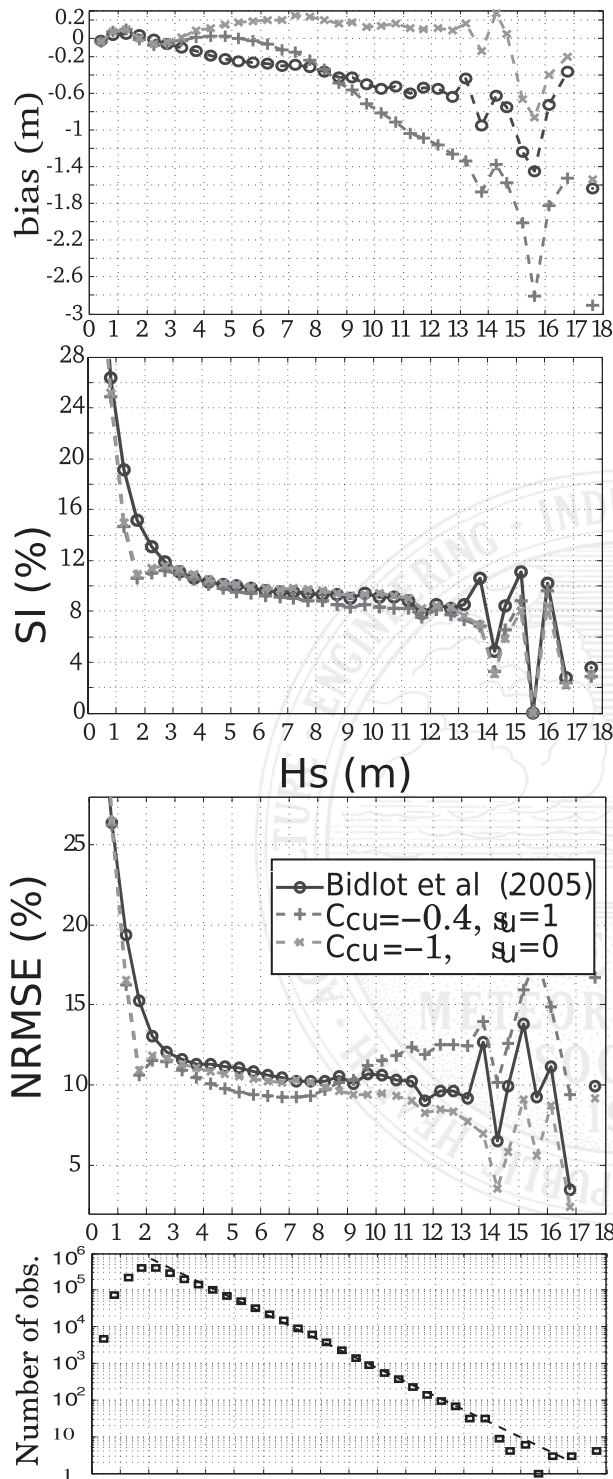


FIG. 10. Wave model errors as a function of observed H_s : (top to bottom) bias, scatter index (SI), NRMSE, and number of observations. The model output at 3-h intervals is compared to that from *Jason-1*, *Envisat*, and *GFO* following the method of Rasche et al. (2008). Namely, the altimeter 1-Hz Ku-band estimates of H_s are averaged over 1° . This provides 2 044 545 observations.

data (Fig. 1), which showed a tendency to underpredict steep swells near the storms and overpredict them in the far field. A simple increase in the swell dissipation was tested but it tended to deteriorate the results of other parameters; this trend is possibly associated with an underestimation of wave heights in the center of severe storms using TEST441. Along European coasts, despite a stronger bias, the errors in T_{m02} are particularly reduced. Again, this reduction of the model scatter can be largely attributed to the decoupling of swell from windsea growth.

The general performance of the parameterizations is synthesized in Table 1. It is interesting to note that the parameterization TEST405, which uses a diagnostic tail for 2.5 times the mean frequency, gives good results in terms of the scatter and bias even for parameters related to short waves (m_3, m_4). This use of a diagnostic tail is thus a reasonable pragmatic alternative to the more costly explicit resolution of shorter waves, which requires a smaller adaptive time step, and more complex parameterizations. The diagnostic tail generally mimics the effects of both the cumulative and sheltering effects. Yet, the parameterization TEST441 demonstrates that it is possible to obtain slightly better results with a free tail. The normalized biases indicated for the mean square slopes are only relative because of the approximate calibration of the radar cross section. They show that the BAJ parameterization (Bidlot et al. 2005), and to a lesser extent the use of a f^{-5} tail, produce energy levels that are relatively lower at high frequency.

b. Lake Michigan

At the global scale, the sea state is never very young, and it is desirable to also verify the robustness of the parameterization in conditions that are more representative of the coastal ocean. We thus follow the analysis of the performance of wave models in Rogers and Wang (2007), hereinafter RW2007, and give results for Lake Michigan, which is representative of relatively young waves. The model was applied with the BAJ, TC, TEST437, and TEST441 parameterizations over the same time frame as was investigated by RW2007: 1 September–14 November 2002. The model is run with 4-km resolution and with other settings and forcing fields similar to those defined by RW2007 (e.g., 10° directional resolution and wind field derived from in situ observations).

Using the directional validation method proposed by these authors, the TC parameterization underestimates the directional spread σ_θ by 1.2° – 1.6° in the range $(0.8$ – $2.0)f_p$, and more at higher frequencies. The underestimation with BAJ is about half, and the TEST441 and TEST437 simulations overpredict the directional spread by about 2.3° – 5.9° in the range $(0.8$ – $2.0)f_p$, and less so for

T1

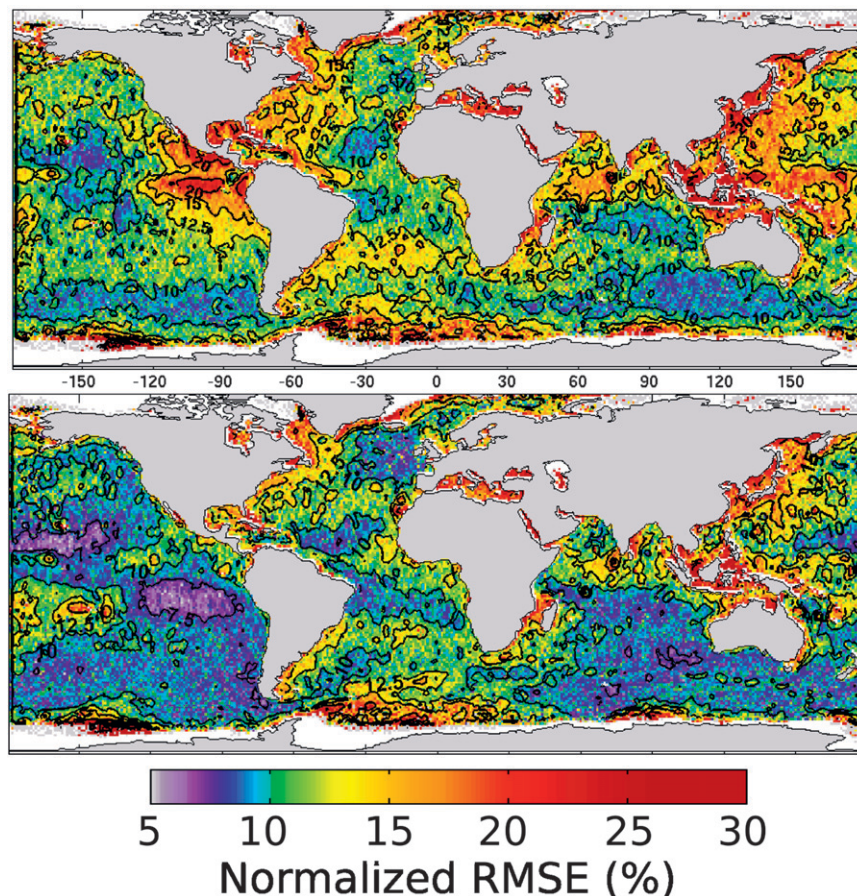


FIG. 11. Normalized RMSE (%) for the significant wave height over the year 2007. The global 0.5° resolution WWATCH model is compared to altimeters aboard the *Jason-1*, *Envisat*, and GFO following the method of Rasche et al. (2008). (top) The result with the BAJ parameterization, and (bottom) the result with the $C_{cu} = -0.4$ and $s_u = 1$ (TEST441) parameterization.

higher frequencies. It thus appears that the broadening introduced to fit the SHOWEX 1999 observations is not optimal for other situations. A similar positive bias in the directional spread is also found in global hindcasts.

T2 F13 Further results are presented in Table 2 and Fig. 13. The top panel in Fig. 13 shows a comparison between the summed values of collocated model and observed spectral densities for the duration of the simulation. This presentation provides a frequency distribution of the bias of the various models, while also indicating the relative contribution of each frequency to the wave climate for this region and time period. The bottom panel in Fig. 13 shows the correlation coefficient r for the equivalent significant wave heights computed for multiple frequency bands. This is presented in terms of f/f_p (bin width = 0.1), with f_p being calculated as the stabilized “synthetic peak frequency” of the corresponding buoy spectrum, as defined in RW2007.

The most noticeable outcome of these comparisons is the relatively poor performance of the TC parameterizations.

Taken in context with other TC results presented herein and a prior undocumented application of the model in the Great Lakes with model wind fields, this suggests that these parameterizations have some undesirable dependence on scale, with the parameters adjusted by Tolman (2002b) being most optimal for ocean-scale applications and nonoptimal for small-scale applications.

The ~~Kiehl-Hack-Hurrell~~ (KHH) physics scheme performs well. This is consistent with prior published applications with the Simulating Waves Nearshore (SWAN) model, (Rogers et al. 2003) and RW2007. However, as noted by those authors, the KHH physics have an advantage in this simple wave climate, and should not be expected to perform well in mixed sea swell conditions.

The BAJ, TEST437 and TEST441 models also perform well here. Taken together with the global comparisons above, we observe no apparent dependency of model skill on the scale of the application with these three physics. In the bias comparison (Fig. 13, top), the BAJ model is

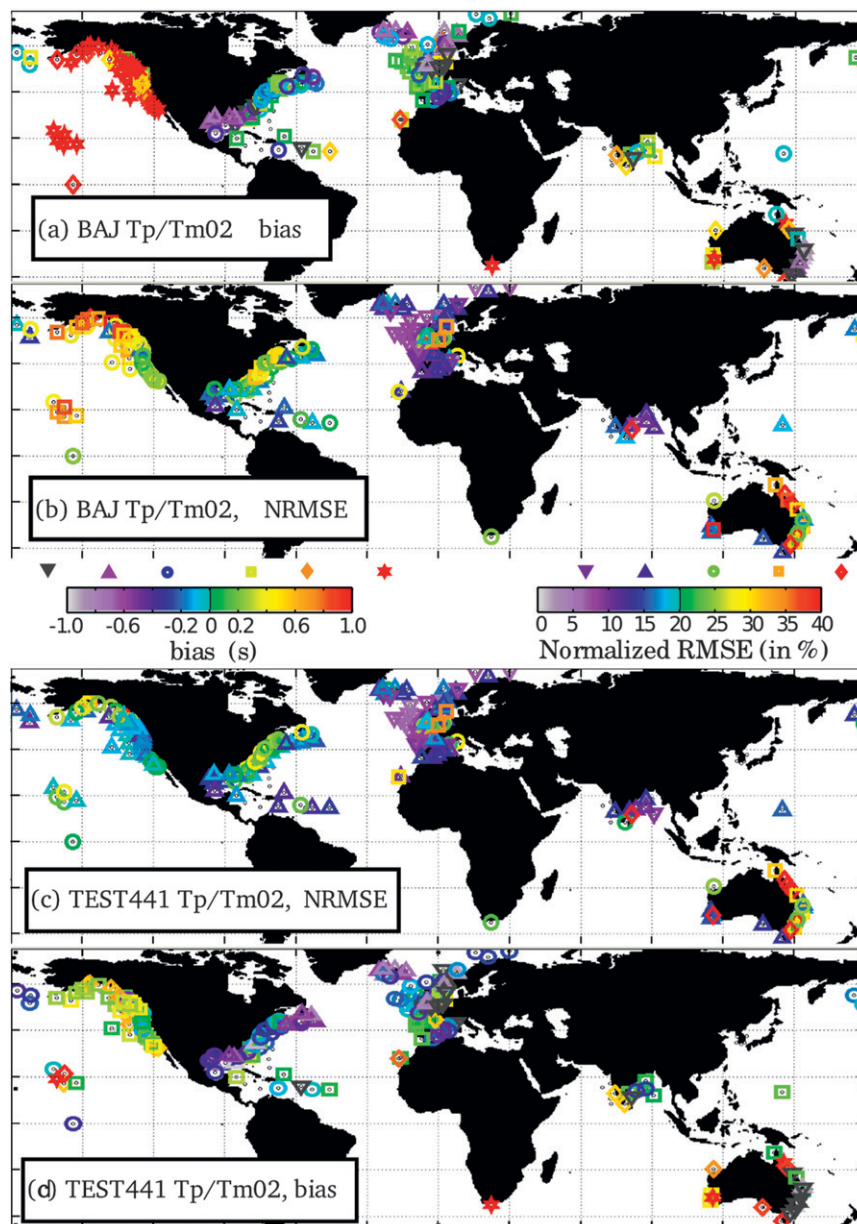


FIG. 12. Statistics for the year 2007 based on the JCOMM verification database (Bidlot et al. 2007b). Shown are the (a),(d) bias and (b),(c) NRMSE for T_p or T_{m02} at in situ locations using (a),(b) the BAJ method or (c),(d) the proposed TEST441 (T_p is shown at all buoys except for the U.K. and French buoys, for which T_{m02} is shown). The different symbols are only used to help distinguish the various colors and do not carry extra information.

nearly identical to the KHH model. Similarly, the two new models are nearly identical. In terms of H_s (Table 2), the TEST441 and TEST437 yield minor underestimations, but give slightly more accurate results compared to observations than BAJ or KHH.

It thus appears that for such young seas, the directional spreading of the parameterization could be improved, but the energy content of various frequency bands, and as

a result the mean period, are reproduced with less scatter than with previous parameterizations.

c. Hurricane Ivan

Although the global hindcast does contain quite a few extreme events, with significant wave heights up to 17 m, these were obtained with a relatively coarse wave model grid and wind forcing (0.5° resolution and 6-h time step)

TABLE 1. The model accuracy for significant wave height measured wave parameters over the oceans in 2007. The mss data from *Jason-1* corresponds to January–July 2007 (393 382 collocated points), while H_s statistics are obtained for the entire year and all available satellites. These global averages are area weighted, and the scatter index (SI) and NRMSE are the area-weighted averages of the local SI and NRMSE. The T_p and T_{m02} statistics are averages of statistics computed for each buoy separately. For T_p , we used WMO buoys 41002, 41010, 42001, 42002, 42003, 44004, 44008, 44011, 44137, 44138, 44139, 44141, 46001, 46004, 46035, 46066, 46184, 46002, 46005, 46036, 46059, 51001, 51002, 51003, and 51004; for T_{m02} , we used 62029, 62081, 62163, and 64045; and for m_3 , we took the results for buoy 46005 as given in Arduin et al.(2009a). Unless otherwise specified by the number in parenthesis, the cutoff frequency is taken to be 0.4 Hz, where C for C band. The normalized bias (NB) is defined as the bias divided by the RMS observed value, while the SI is defined as the RMS difference between the modeled and observed values, after correction for the bias, normalized by the RMS observed value, and r is Pearson’s correlation coefficient.

	BAJ	Test 405	Test 437	Test 441
H_s				
NB (%)	-2.1	-0.8	0.2	-1.23
SI (%)	11.8	10.5	10.6	10.4
NRMSE (%)	13.0	11.5	11.6	11.3
m_4 (C)				
NB (%)	-16.1	-4.9	-2.3	-2.5
SI (%)	10.7	9.1	9.1	9.1
R	0.867	0.925	0.931	0.939
T_p				
NRMSE (%)	24.1	19.0	19.4	18.2
T_{m02}				
NRMSE (%)	7.6	6.9	6.6	6.7
m_3				
NB (%)	-14.6	1.7	-2.3	-2.4
SI (%)	20.6	12.6	14.8	12.6
NRMSE (%)	25.3	13.1	13.1	12.8
R	0.934	0.971	0.961	0.973

that are insufficient to resolve small storms such as tropical cyclones (Tolman and Alves 2005). Hurricane waves do share many similarities with more usual sea states (Young 2006), but the high winds and their rapid rotation are particularly challenging for numerical wave models. It is thus necessary to verify that the new source functions perform adequately under extreme wind conditions. A simulation of Hurricane Ivan (Gulf of Mexico, September 2004) is chosen for this purpose because it was extensively measured (e.g., Wang et al. 2005) and hindcasted.

Winds for this simulation are based on 3-hourly gridded surface wind analyses created by National Oceanic and Atmospheric Administration’s (NOAA) Hurricane Research Division (HRD). As an intermediate step, fields are reprocessed at 30-min intervals, with the storm position updated at each interval (thus, semi-Lagrangian interpolation). The wind speeds are reduced by factor of 1/1.11 to convert from the maximum sustained gust to an

TABLE 2. Model–data comparison at NDBC buoy 45007 (Lake Michigan) for four frequency bands. Statistics are given for equivalent significant wave heights in the bands $0.5f_p < f < 0.8f_p$ (band 1), $0.8f_p < f < 1.2f_p$ (band 2), $1.2f_p < f < 2f_p$ (band 3), and $2f_p < f < 3f_p$ (band 4). The KHH $n = 2$ run corresponds to the dissipation parameterization defined by Rogers et al. (2003) and based on Komen et al. (1984) and applied in the WWATCH code. For the peak frequency band, statistics are also given for the directional spread σ_θ .

	BAJ	TC	Test 437	Test 441	KHH $n = 2$
H_s band 1					
SI (%)	76	71	77	82	76
H_s band 2					
SI (%)	16	19	15	15	15
H_s band 3					
SI (%)	18	26	17	17	19
H_s band 4					
SI (%)	20	32	18	17	22
σ_θ band 2					
SI (%)	22	24	30	30	25
Bias (°)	-0.4	-1.6	2.3	2.6	0.8
H_s bias (m)	-0.03	-0.11	-0.02	-0.02	0.04
R	0.95	0.94	0.96	0.96	0.96
SI (%)	19	25	18	18	19
T_{m02}					
Bias (s)	0.02	-0.39	-0.05	-0.05	0.01
R	0.89	0.87	0.90	0.90	0.90
SI (%)	10	14	9	9	10

hourly mean. The HRD winds do not cover the entire computational domain. For areas falling outside the domain, the nearest National Data Buoy Center (NDBC) wind observation is used. This produces some non-physical spatial discontinuities in the wind field, but these

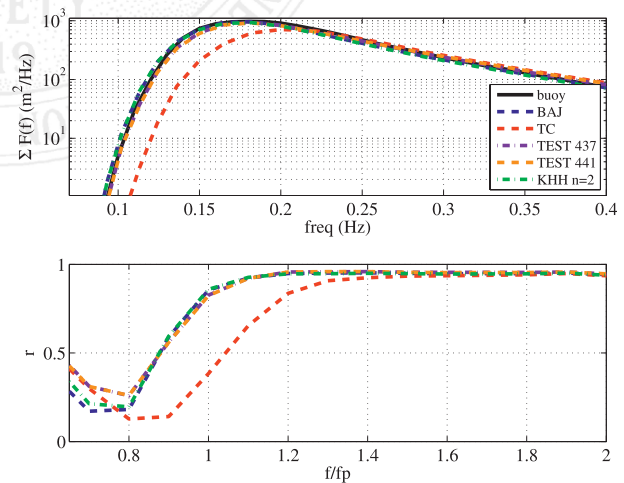


FIG. 13. Model–data comparison at NDBC buoy 45007 (Lake Michigan). (top) Comparison of the summed spectral density vs the frequency for the duration of the simulation, and (bottom) the correlation coefficients vs the normalized frequency (see text for explanation).

are smoothed in the wave model integration and, in any event, only affect weaker wind seas far from the storm center.

Bathymetry is taken from the Naval Research Laboratory's 2'-resolution database (DBDB2) coarsened to the computational grid resolution (0.1°). The directional resolution is 10°, and the frequency range is limited to 0.0418–0.4117 Hz. The model was applied from 13 to 16 September 2004. Model results are illustrated in Fig. 14. The models were validated at all of the buoys in the Gulf of Mexico. Results from buoy 42040, where the waves were largest, are shown here.

F14

Model runs with parameterizations BAJ, TEST437, and TEST441 give very similar results: close to the observations, except for the highest waves ($H_s > 13$ m at buoy 42040), where TEST437 and TEST441 give slightly smaller values. Results with the TC parameterization are generally lower in terms of H_s than are all of the parameterizations that share a Janssen type of input. It appears that the new source term perform similarly to BAJ and is able to reproduce such young waves and severe sea states.

Because the wind forcing enters the wave model through a wind stress parameterized in a way that may not apply to such conditions, it is worthwhile to reexamine some choices made above. In particular the surface roughness was allowed to exceed 0.002 in TEST441b, which resulted in better estimates of H_s . Lifting this constraint shows that, for these very high winds, the wind-sheltering effect plays a similar role in limiting the roughness to $z_{0,max}$, with the difference that it tends to narrow the wind input spectrum (Fig. 7). This narrower wind input has a limited effect of the wind stress and H_s , but is has a noticeable effect on the spectral shape. This is illustrated by the low-frequency energy that appears to be strongly overestimated before the peak of the storm for TEST441b. In general the new parameterizations provide results that are as reasonable as those of previous parameterizations, given the uncertainty of the wind forcing.

5. Conclusions

A set of parameterizations for the dissipation source terms of the wave energy balance equation have been proposed, based on known properties of swell dissipation and wave breaking statistics. This dissipation includes an explicit nonlinear swell dissipation and a wave breaking parameterization that contains a cumulative term, representing the dissipation of short waves by longer breakers, and different dissipation rates for different directions. These dissipation parameterizations have been combined with a modified form of the wind input proposed by Janssen (1991), in which the questionable

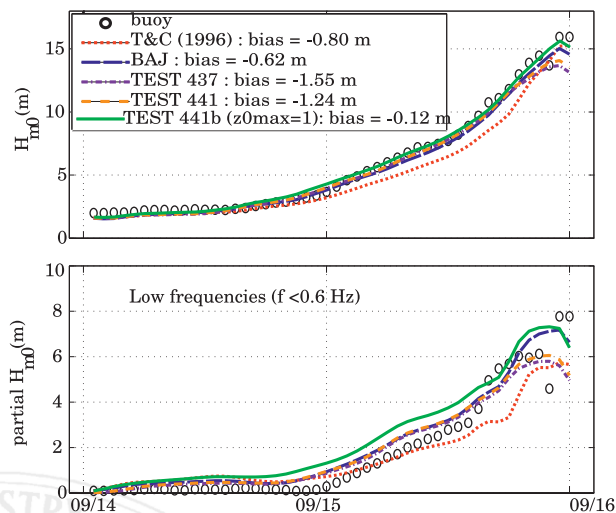


FIG. 14. Time series of model and buoy (top) significant wave height and (bottom) partial wave height (for $f < 0.06$ Hz), during the passage of Hurricane Ivan, at buoy 42040. The 10-m discus buoy was capsized by waves and could not record waves after 16 September.

gustiness parameter z_α has been reduced, and the general shape of the wind input has been significantly modified. The resulting source term balance is thus markedly different from the previous proposed forms, with a near balance for very old seas between the air–sea friction term that dissipates swell and the nonlinear energy flux to low frequencies. Also, the wind input is concentrated in a narrower range of frequencies.

For younger seas the wind input is weaker than that given by Janssen (1991) but stronger than that given by Tolman and Chalikov (1996). However, the dissipation at the peak is generally stronger because it is essentially based on a local steepness and these dominant waves are the steepest in the sea state. As a result, the short fetch growth is relatively weaker than that with the source term combination proposed by Bidlot et al. (2007a) (BAJ). The choice of parameters tested here tends to produce broader directional spectra than those observed in Lake Michigan and global hindcasts, and slanting fetch directions that are too oblique relative to the wind (Fig. 2). In this respect the new source terms are intermediate between BAJ and TC.

Another defect comes from the definition of the saturation level used to define the breaking-induced dissipation. Here, as in the work by van der Westhuysen et al. (2007), the saturation is local in frequency space, whereas wave breaking is naturally expected to have a relatively broad impact due to its localization in space and time (Hasselmann 1974). This is expected to produce an overestimation of the energy just below the peak, and an underestimation at the peak of the saturation spectrum.



TABLE A1. Wind–wave interaction parameters as implemented in version 3.14 of SHOM in the WWATCH code, and values used in the tests presented here. In WWATCH, all parameters are accessible via the `SIN3` name-list. All of these parameters are included in version 3.14 of WWATCH. Note that s_0 is a switch that, if nonzero, activates the calculation of S_{out} .

Parameter	Eq.	Variable in WWATCH	WAM cycle 4	BAJ	TEST405	TEST437	TEST441
α_0	(19)	ALPHA0	0.01	0.0095	—	—	—
β_{max}	(20)	BETAMAX	1.2	1.2	1.55	1.52	—
z_α	(20)	ZALP	0.011	0.011	0.006	—	—
$z_{0, max}$	(22)	ZOMAX	NA	NA	0.002	—	—
s_u	(24)	TAUWSHELTER	0.0	0.0	0.0	0.0	1.0
s_0		SWELLFPAR	0	0	3	—	—
s_1	(10)	SWELLF	0.0	0.0	0.8	—	—
s_2	(10)	SWELLF2	0.0	0.0	−0.018	—	—
s_3	(10)	SWELLF3	0.0	0.0	0.015	—	—
$0.5Re_c H_s$		SWELLF4	0.0	1×10^5	—	—	—
C_{dsv}	(9)	SWELLF5	0.0	0.0	1.2	—	—
r_{z0}	(11)	ZORAT	0.0	0.0	0.04	—	—
z_u	(21)	ZWND	10	10	10	10	10
p	(19)	SINTHP	2	2	2	2	2

These effects likely contribute to the persistent over-estimation of low-frequency energy in the model.

In spite of these defects, the new parameterization produces robust results and clearly outperforms the Bidlot et al. (2007a) parameterization in global hindcasts, whether one considers dominant wave parameters, H_s , T_{m02} , and T_p or parameters sensitive to the high-frequency content, such as the surface Stokes U_{ss} drift or the mean square slope. At global scales, errors in H_s , T_p , and U_{ss} are—on average—reduced by 15%, 25%, and 50% relative to those obtained with the parameterization by Bidlot et al. (2007a). Global and regional hindcasts (North and Irish Seas, English Channel, Tuamotu, Lesser Antilles, and more), from 2002 to 2010 at least, are available for further analysis [online](http://tinyurl.com/yetsofy) (<http://tinyurl.com/yetsofy>).

Another important aspect of this study was the validation at regional to global scales. ~~We note that the TC paper does include verification with steady-state, fetch-limited growth curves. Though such verification is a useful step, the outcome of the Lake Michigan hindcast suggests that such verification gives no indication of the model’s skill in real subregional-scale applications. One of the parameterizations proposed here (TEST441) also gives slightly poorer performance for young seas, which is not obvious in the case of Lake Michigan, but was revealed by hindcasts of Mediterranean waves (not shown).~~

Because our intention was only to demonstrate the capability of new dissipation parameterizations and the resulting source term balances, we have not fully adjusted the 18 parameters that define the deep water parameterizations, compared to the roughly 9 used by Bidlot et al. (2007a). The results presented here are thus preliminary in terms of model performance, which is why the parameterizations are still given temporary names

like TEST441. As illustrated by the Hurricane Ivan hindcast, some parameters, such as $z_{0,max}$, are probably unnecessary; in that particular case, the removal of $z_{0,max}$ improved the results, but for global-scale results it had no impact at all (not shown).

Because five of the extra parameters define the air–sea friction term that produces swell dissipation, and two define the cumulative breaking term, it is feasible to define a systematic adjustment procedure that should increase the model accuracy by separately adjusting the swell, wind sea peak, and high-frequency properties. In particular, the directional distribution may be improved by making the dissipation term more isotropic (i.e., taking $\delta_d > 0.3$) or modifying the definition of the saturation parameter B' in Eq. (12). In a forthcoming paper we shall further investigate the responses of the wave field to varying currents, from global scales to regional tidal currents. From that research, we expect that wave steepening will produce much more dissipation due to breaking, as envisaged by Phillips (1984).

Obviously, it is well known that the discrete interaction approximation used here to compute the nonlinear interactions is the source of large errors, and further calculations will be performed using a more accurate estimation of these interactions in the future.

Acknowledgments. This research would not have been possible without the dedication of Hendrik Tolman, Henrique Alves, and Arun Chawla in putting together the core of the WAVEWATCH-III code. Florent Birrien performed the integration of Aaron Roland’s routines into the WWATCH framework. Wind and wave data were kindly provided by ECMWF, Météo-France, and the French Centre d’Etudes Techniques Maritimes Et Fluviales (CETMEF). The SHOM buoy deployments

TABLE A2. Dissipation parameters as implemented in version 3.14 of SHOM in the WWATCH code, and values used in the tests presented here. In WWATCH, all parameters are accessible via the SDS3 name-list. The only parameters not defined in the present paper are C_{lf} and C_{hf} , which act like switches to activate the BAJ parameterization for the part of the spectrum with saturation below and above the spectrum, respectively. Most of these parameters are also included in version 3.14, except for C_{cu} , which is needed for TEST437 and TEST441 with results described here. The TEST405 can be run with version 3.14. The parameter M_0 is a switch for the correction or not of B_r into B'_r , when $M_0 = 1$, as is the case here, the correction is not applied.

Parameter	Eq.	Variable in WWATCH	WAM4	BAJ	TEST405	TEST437	TEST441	TEST443
C_{ds}	(2)	SDSC1	-4.5	-2.1	0.0	—	—	—
r	(2)	WNMEANP	-0.5	0.5	0.5	—	—	—
f_{FM}	(7)	FXFM3	2.5	2.5	2.5	9.9	—	—
δ_1	(2)	SDSDELTA1	0.5	0.4	0.0	—	—	—
δ_2	(2)	SDSDELTA2	0.5	0.6	0.0	—	—	—
C_{ds}^{sat}	(13)	SDSC2	0.0	0.0	-2.2×10^{-5}	—	—	—
C_{lf}		SDSLF	1.0	1.0	0.0	—	—	—
C_{hf}		SDSHF	1.0	1.0	0.0	—	—	—
Δ_θ	(12)	SDSDTH	0.0	0.0	80	—	—	—
B_r	(12)	SDSBR	0.0	0.0	1.2×10^{-3}	9×10^{-4}	—	—
r_{cu}	(18)	SDSBRF1	0.0	0.0	0.0	0.5	—	—
$2 \times C_{cu}$	(18)	SDSC3	0.0	0.0	0.0	-2.0	-0.8	—
s_B	(12)	SDSCOS	0.0	0.0	0.0	2.0	—	—
δ_d	(13)	SDSDC6	0.0	0.0	1.0	0.3	0.3	0.0
M_0		SDSBM0	0.0	0.0	1.0	—	—	—
M_1		SDSBM1	0.0	0.0	0.2428	—	—	—
M_2		SDSBM2	0.0	0.0	1.9995	—	—	—
M_3		SDSBM3	0.0	0.0	-2.5709	—	—	—
M_4		SDSBM4	0.0	0.0	1.3286	—	—	—

were managed by David Corman with invaluable help from Guy Amis. Wave data were kindly provided by the U.S. Navy, ESA, and CNES, and the many in situ contributors to the JCOMM (WMO-IOC) exchange program coordinated by Jean-Raymond Bidlot.

may require a retuning of the wind source function, which can be performed by a readjustment of β_{max} .

APPENDIX

Parameter Settings

The numerical values of all parameters that define the source functions are listed in Table A1 for the wind-wave interaction term S_{atm} and Table A2 for the wave-ocean interaction term S_{oc} . We also recall that the nonlinear coupling coefficient (variable NLPROP in WWATCH) is set to 2.78×10^7 in all cases, except for the two parameterizations mostly frequently used here, with $C_{nl} = 2.5 \times 10^7$ in TEST437 and TEST441. Although the best performance for most parameters is obtained with the TEST441 settings, its underestimation of extreme sea states may be a problem in some applications for which TEST437 may be preferred. A full tuning of the model has not been attempted yet and it is possible that simple adjustments to β_{max} , C_{cu} , r_{cu} , and s_u may produce even better results. Finally, these parameters have been mostly adjusted for deep water conditions using European Centre for Medium-Range Weather Forecasts (ECMWF) winds. Using other sources of winds for large-scale applications

REFERENCES

- Alves, J. H. G. M., and M. L. Banner, 2003: Performance of a saturation-based dissipation-rate source term in modeling the fetch-limited evolution of wind waves. *J. Phys. Oceanogr.*, **33**, 1274–1298.
- , —, and I. R. Young, 2003: Revisiting the Pierson–Moskowitz asymptotic limits for fully developed wind waves. *J. Phys. Oceanogr.*, **33**, 1301–1323.
- Ardhuin, F., and A. D. Jenkins, 2005: On the effect of wind and turbulence on ocean swell. *Proc. 15th Int. Polar and Offshore Engineering Conf.*, Vol. III, Seoul, South Korea, ISOPE, 429–434.
- , and —, 2006: On the interaction of surface waves and upper-ocean turbulence. *J. Phys. Oceanogr.*, **36**, 551–557.
- , and A. Le Boyer, 2006: Numerical modelling of sea states: Validation of spectral shapes (in French). *Navigation*, **54**, 55–71.
- , T. H. C. Herbers, K. P. Watts, G. P. van Vledder, R. Jessen, and H. Graber, 2007: Swell and slanting fetch effects on wind wave growth. *J. Phys. Oceanogr.*, **37**, 908–931.
- , F. Collard, B. Chapron, P. Queffelecoul, J.-F. Filipot, and M. Hamon, 2008a: Spectral wave dissipation based on observations: a global validation. *Proc. Chinese–German Joint Symp. on Hydraulics and Ocean Engineering*, Darmstadt, Germany, 391–400.
- , N. Rasche, and K. A. Belibassakis, 2008b: Explicit wave-averaged primitive equations using a generalized Lagrangian mean. *Ocean Modell.*, **20**, 35–60, doi:10.1016/j.ocemod.2007.07.001.
- , B. Chapron, and F. Collard, 2009a: Observation of swell dissipation across oceans. *Geophys. Res. Lett.*, **36**, L06607, doi:10.1029/2008GL037030.



- , L. Marié, N. Rasche, P. Forget, and A. Roland, 2009b: Observation and estimation of Lagrangian, Stokes, and Eulerian currents induced by wind and waves at the sea surface. *J. Phys. Oceanogr.*, **39**, 2820–2838.
- AU6** Babanin, A. V., and I. R. Young, 2005: Two-phase behaviour of the spectral dissipation of wind waves. *Proc. Fifth Int. Symp. Ocean Wave Measurement and Analysis*, Madrid, Spain, ASCE, Paper 51.
- , and A. J. van der Westhuysen, 2008: Physics of saturation-based dissipation functions proposed for wave forecast models. *J. Phys. Oceanogr.*, **38**, 1831–1841.
- Babanin, A., I. Young, and M. Banner, 2001: Breaking probabilities for dominant surface waves on water of finite depth. *J. Geophys. Res.*, **106**, 11 659–11 676.
- , K. Tsagareli, I. Young, and D. Walker, 2007: Implementation of new experimental input/dissipation terms for modelling spectral evolution of wind waves. *Proc. 10th Int. Workshop on Wave Hindcasting and Forecasting*, Oahu, HI, WMO/IOC Joint Technical Commission for Oceanography and Marine Meteorology (JCOMM), C2. [Available online at <http://www.waveworkshop.org/10thWaves/ProgramFrameset.htm>.]
- Banner, M. L., and I. R. Young, 1994: Modeling spectral dissipation in the evolution of wind waves. Part I: Assessment of existing model performance. *J. Phys. Oceanogr.*, **24**, 1550–1570.
- , and R. P. Morison, 2006: On modeling spectral dissipation due to wave breaking for ocean wind waves. *Proc. Ninth Int. Workshop on Wave Hindcasting and Forecasting*, Victoria, BC, Canada, JCOMM. [Available online at <http://www.waveworkshop.org/9thWaves/ProgramFrameset.htm>.]
- , and W. L. Peirson, 2007: Wave breaking onset and strength for two-dimensional deep-water wave groups. *J. Fluid Mech.*, **585**, 93–115.
- , I. S. F. Jones, and J. C. Trinder, 1989: Wavenumber spectra of short gravity waves. *J. Fluid Mech.*, **198**, 321–344.
- , A. V. Babanin, and I. R. Young, 2000: Breaking probability for dominant waves on the sea surface. *J. Phys. Oceanogr.*, **30**, 3145–3160.
- , J. R. Gemmrich, and D. M. Farmer, 2002: Multiscale measurement of ocean wave breaking probability. *J. Phys. Oceanogr.*, **32**, 3364–3374.
- Barber, N. F., 1949: Behaviour of waves on tidal streams. *Proc. Roy. Soc. London*, **198A**, 81–93.
- Bidlot, J.-R., 2008: Intercomparison of operational wave forecasting systems against buoys: Data from ECMWF, Met Office, FNMO, NCEP, DWD, BoM, SHOM and JMA, September 2008 to November 2008. JCOMM Tech. Rep., 66 pp. [Available online at http://www.jcomm-services.org/modules/documents/documents/model_comparison_second_list_200809_200811.pdf.]
- , S. Abdalla, and P. Janssen, 2005: A revised formulation for ocean wave dissipation in CY25R1. Research Dept. Tech. Rep. Memo. R60.9/JB/0516, ECMWF, Reading, United Kingdom.
- AU7** —, P. Janssen, and S. Abdalla, 2007a: A revised formulation of ocean wave dissipation and its model impact. ECMWF Tech. Rep. Memo. 509, Reading, United Kingdom.
- , and Coauthors, 2007b: Inter-comparison of operational wave forecasting systems. *Proc. 10th Int. Workshop on Wave Hindcasting and Forecasting*, Oahu, HI, JCOMM. [Available online at <http://www.waveworkshop.org/10thWaves/ProgramFrameset.htm>.]
- AU8** Cavaleri, L., 2006: Wave modeling where to go in the future. *Bull. Amer. Meteor. Soc.*, **87**, 207–214.
- , 2009: Wave modeling—Missing the peaks. *J. Phys. Oceanogr.*, **39**, 2757–2778.
- Chalikov, D. V., 1993: Comments on “Wave-induced stress and the drag of air flow over sea waves” and “Quasi-linear theory of wind-wave generation applied to wave forecasting.” *J. Phys. Oceanogr.*, **23**, 1597–1600.
- AU17** —, and M. Y. Belevich, 1993: One-dimensional theory of the wave boundary layer. *Bound.-Layer Meteor.*, **63**, 65–96.
- Chen, G., and S. E. Belcher, 2000: Effects of long waves on wind-generated waves. *J. Phys. Oceanogr.*, **30**, 2246–2256.
- Collard, F., A. Mouche, B. Chapron, C. Danilo, and J. Johannessen, 2008: Routine high resolution observation of selected major surface currents from space. *Proc. SEASAR 2008*, ESA–ESRIN, Frascati, Italy, SP-656. [Available online at http://earth.esa.int/workshops/seasar2008/participants/287/pres_287_Collard.pdf.]
- , F. Ardhuin, and B. Chapron, 2009: Monitoring and analysis of ocean swell fields using a spaceborne SAR: A new method for routine observations. *J. Geophys. Res.*, **114**, C07023, doi:10.1029/2008JC005215.
- Dalrymple, R. A., 1974: A finite amplitude wave on a linear shear current. *J. Geophys. Res.*, **79**, 4498–4504.
- Darbyshire, J., 1958: The generation of waves by wind. *Philos. Trans. Roy. Soc. London*, **215A**, 299–428.
- Dobson, F., W. Perrie, and B. Toulany, 1989: On the deep water fetch laws for wind-generated surface gravity waves. *Atmos.–Ocean*, **27**, 210–236.
- Donelan, M. A., 1998: Air-water exchange processes. *Physical Processes in Lakes and Oceans*, J. Imberger, Ed., Amer. Geophys. Union, 18–36.
- Dore, B. D., 1978: Some effects of the air–water interface on gravity waves. *Geophys. Astrophys. Fluid Dyn.*, **10**, 215–230.
- Filipot, J.-F., F. Ardhuin, and A. Babanin, 2010: A unified deep-to-shallow-water spectral wave breaking dissipation formulation. Part I. Breaking probability. *J. Geophys. Res.*, **115**, in press.
- AU9** Gelci, R., H. Cazalé, and J. Vassal, 1957: Prédiction de la houle. La méthode des densités spectroangulaires. *Bull. Inform. Com. Océanogr. Etude Côtes*, **9**, 416–435.
- Gemmrich, J. R., M. L. Banner, and C. Garrett, 2008: Spectrally resolved energy dissipation rate and momentum flux of breaking waves. *J. Phys. Oceanogr.*, **38**, 1296–1312.
- Gourrion, J., D. Vandemark, S. Bailey, and B. Chapron, 2002: Investigation of C-band altimeter cross section dependence on wind speed and sea state. *Can. J. Remote Sens.*, **28**, 484–489.
- Grant, W. D., and O. S. Madsen, 1979: Combined wave and current interaction with a rough bottom. *J. Geophys. Res.*, **84**, 1797–1808.
- Hargreaves, J. C., and J. D. Annan, 2000: Comments on improvement of the short-fetch behavior in the Wave Ocean Model (WAM). *J. Atmos. Oceanic Technol.*, **18**, 711–715.
- Harris, D. L., 1966: The wave-driven wind. *J. Atmos. Sci.*, **23**, 688–693.
- Hasselmann, K., 1971: On the mass and momentum transfer between short gravity waves and larger-scale motions. *J. Fluid Mech.*, **4**, 189–205.
- , 1974: On the spectral dissipation of ocean waves due to white capping. *Bound.-Layer Meteor.*, **6**, 107–127.
- Hasselmann, S., K. Hasselmann, J. Allender, and T. Barnett, 1985: Computation and parameterizations of the nonlinear energy transfer in a gravity-wave spectrum. Part II: Parameterizations of the nonlinear energy transfer for application in wave models. *J. Phys. Oceanogr.*, **15**, 1378–1391.
- Högström, U., A. Smedman, E. Sahleé, H. Pettersson, and F. Zhang, 2009: The atmospheric boundary layer during swell: A field study and interpretation of the turbulent kinetic energy budget for high wave ages. *J. Atmos. Sci.*, **66**, 2764–2779.

- Janssen, P. A. E. M., 1991: Quasi-linear theory of wind wave generation applied to wave forecasting. *J. Phys. Oceanogr.*, **21**, 1631–1642.
- , 2009: On some consequences of the canonical transformation in the Hamiltonian theory of water waves. *J. Fluid Mech.*, **637**, 1–44.
- , K. Hasselmann, S. Hasselmann, and G. J. Komen, 1994: Parametrization of source terms and the energy balance in a growing wind sea. *Dynamics and Modelling of Ocean Waves*, G. J. Komen et al., Eds., Cambridge University Press, 215–238.
- , O. Saetra, C. Wettre, and H. Hersbach, 2004: Impact of the sea state on the atmosphere and ocean. *Ann. Hydrogr.*, **3**, 3-1–3-23.
- Jensen, B. L., B. M. Sumer, and J. Fredsøe, 1989: Turbulent oscillatory boundary layers at high Reynolds numbers. *J. Fluid Mech.*, **206**, 265–297.
- Komen, G. J., K. Hasselmann, and S. Hasselmann, 1984: On the existence of a fully developed windsea spectrum. *J. Phys. Oceanogr.*, **14**, 1271–1285.
- , L. Cavaleri, M. Donelan, K. Hasselmann, S. Hasselmann, and P. A. E. M. Janssen, 1994: *Dynamics and Modelling of Ocean Waves*. Cambridge University Press, 554 pp.
- Lefèvre, J.-M., S. E. Ștefănescu, and V. Makin, 2004: Implementation of new source terms in a third generation wave model. Preprints, *Third Int. Workshop on Wave Hindcasting and Forecasting*, Montreal, QC, Canada, Environment Canada.
- AU10** Long, C. E., and D. T. Resio, 2007: Wind wave spectral observations in Currituck Sound, North Carolina. *J. Geophys. Res.*, **112**, C05001, doi:10.1029/2006JC003835.
- Longuet-Higgins, M. S., and J. S. Turner, 1974: An ‘entraining plume’ model of a spilling breaker. *J. Fluid Mech.*, **63**, 1–20.
- Magne, R., K. Belibassakis, T. H. C. Herbers, F. Ardhuin, W. C. O’Reilly, and V. Rey, 2007: Evolution of surface gravity waves over a submarine canyon. *J. Geophys. Res.*, **112**, C01002, doi:10.1029/2005JC003035.
- Makin, V. K., and M. Stam, 2003: New drag formulation in NEDWAM. KNMI Tech. Rep. 250, Koninklijk Nederlands Meteorologisch Instituut, De Bilt, Netherlands.
- AU11** Manasseh, R., A. V. Babanin, C. Forbes, K. Rickards, I. Bobevski, and A. Ooi, 2006: Passive acoustic determination of wave-breaking events and their severity across the spectrum. *J. Atmos. Oceanic Technol.*, **23**, 599–618.
- Melville, W. K., F. Verron, and C. J. White, 2002: The velocity field under breaking waves: Coherent structures and turbulence. *J. Fluid Mech.*, **454**, 203–233.
- Munk, W. H., and M. A. Traylor, 1947: Refraction of ocean waves: A process linking underwater topography to beach erosion. *J. Geol.*, **LV**, 1–26.
- Peirson, W. L., and M. L. Banner, 2003: Aqueous surface layer flows induced by microscale breaking wind waves. *J. Fluid Mech.*, **479**, 1–38.
- Phillips, O. M., 1958: The equilibrium range in the spectrum of wind-generated waves. *J. Fluid Mech.*, **4**, 426–433.
- , 1963: On the attenuation of long gravity waves by short breaking waves. *J. Fluid Mech.*, **16**, 321–332.
- , 1984: On the response of short ocean wave components at a fixed wavenumber to ocean current variations. *J. Phys. Oceanogr.*, **14**, 1425–1433.
- , 1985: Spectral and statistical properties of the equilibrium range in wind-generated gravity waves. *J. Fluid Mech.*, **156**, 505–531.
- Pierson, W. J., Jr., and L. Moskowitz, 1964: A proposed spectral form for fully developed wind seas based on the similarity theory of S. A. Kitaigorodskii. *J. Geophys. Res.*, **69**, 181–185, 190.
- Polnikov, V. G., and V. Inocentini, 2008: Comparative study of performance of wind wave model: Wavewatch modified by new source function. *Eng. Appl. Comput. Fluid Mech.*, **2**, 466–481.
- Queffelec, P., and D. Croizé-Fillon, 2008: Global altimeter SWH data set, version 4, october 2008. Ifremer Tech. Rep., 13 pp. [Available online at ftp://ftp.ifremer.fr/ifremer/cersat/products/swath/altimeters/waves/documentation/altimeter_wave_merge_4.0.pdf.]
- Rasche, N., F. Ardhuin, P. Queffelec, and D. Croizé-Fillon, 2008: A global wave parameter database for geophysical applications. Part 1: Wave-current–turbulence interaction parameters for the open ocean based on traditional parameterizations. *Ocean Modell.*, **25**, 154–171, doi:10.1016/j.ocemod.2008.07.006.
- Rogers, W. E., and D. W. C. Wang, 2007: Directional validation of wave predictions. *J. Atmos. Oceanic Technol.*, **24**, 504–520.
- , P. A. Hwang, and D. W. Wang, 2003: Investigation of wave growth and decay in the SWAN model: Three regional-scale applications. *J. Phys. Oceanogr.*, **33**, 366–389.
- Ruessink, B. G., D. J. R. Walstra, and H. N. Southgate, 2003: Calibration and verification of a parametric wave model on barred beaches. *Coastal Eng.*, **48**, 139–149.
- Smedman, A., U. Höglström, E. Sahleé, W. M. Drennan, K. K. Kahma, H. Pettersson, and F. Zhang, 2009: Observational study of marine atmospheric boundary layer characteristics during swell. *J. Atmos. Sci.*, **66**, 2747–2763.
- Stansell, P., and C. MacFarlane, 2002: Experimental investigation of wave breaking criteria based on wave phase speeds. *J. Phys. Oceanogr.*, **32**, 1269–1283.
- Tolman, H. L., 1992: Effects of numerics on the physics in a third-generation wind-wave model. *J. Phys. Oceanogr.*, **22**, 1095–1111.
- , 2002a: Limiters in third-generation wind wave models. *Global Atmos. Oceanic Syst.*, **8**, 67–83.
- , 2002b: Validation of WAVEWATCH-III version 1.15. NOAA/NWS/NCEP/MMAB Tech. Rep. 213, 33 pp.
- , 2003: Treatment of unresolved islands and ice in wind wave models. *Ocean Modell.*, **5**, 219–231.
- , 2007: The 2007 release of WAVEWATCH III. *Proc. 10th Int. Workshop of Wave Hindcasting and Forecasting*, Oahu, HI, JCOMM, Q4. [Available online at http://www.waveworkshop.org/10thWaves/ProgramFrameset.htm.]
- , 2008: A mosaic approach to wind wave modeling. *Ocean Modell.*, **25**, 35–47, doi:10.1016/j.ocemod.2008.06.005.
- , 2009: User manual and system documentation of WAVEWATCH-III version 3.14. NOAA/NWS/NCEP/MMAB Tech. Rep. 276.
- AU12** —, and D. Chalikov, 1996: Source terms in a third-generation wind wave model. *J. Phys. Oceanogr.*, **26**, 2497–2518.
- , and J.-H. G. M. Alves, 2005: Numerical modeling of wind waves generated by tropical cyclones using moving grids. *Ocean Modell.*, **9**, 305–323.
- Tournadre, J., K. Whitmer, and F. Girard-Ardhuin, 2008: Iceberg detection in open water by altimeter waveform analysis. *J. Geophys. Res.*, **113**, C08040, doi:10.1029/2007JC004587.
- Tsagareli, K., 2008: Numerical investigation of wind input and spectral dissipation in evolution of wind waves. Ph.D. thesis, University of Adelaide, Adelaide, SA, Australia.
- AU13** Tulin, M. P., and M. Landrini, 2001: Breaking waves in the ocean and around ships. *Proc. 23rd ONR Symp. on Naval Hydrodynamics*, Val de Reuil, France, Naval Studies Board, 713–745.
- Vandemark, D., P. D. Mourad, S. A. Bailey, T. L. Crawford, C. A. Vogel, J. Sun, and B. Chapron, 2001: Measured changes in ocean surface roughness due to atmospheric boundary layer rolls. *J. Geophys. Res.*, **106**, 4639–4654.

- , B. Chapron, J. Sun, G. H. Crescenti, and H. C. Graber, 2004: Ocean wave slope observations using radar backscatter and laser altimeters. *J. Phys. Oceanogr.*, **34**, 2825–2842.
- van der Westhuysen, A. J., 2007: Advances in the spectral modelling of wind waves in the nearshore. Ph.D. thesis, Delft University of Technology, Delft, Netherlands, 206 pp.
- , M. Zijlema, and J. A. Battjes, 2007: Saturation-based whitecapping dissipation in SWAN for deep and shallow water. *Coastal Eng.*, **54**, 151–170.
- van Vledder, G. P., and D. P. Hurdle, 2002: Performance of formulations for whitecapping in wave prediction models. *Proc. OMAE.02 21st Int. Conf. on Offshore Mechanics and Arctic Engineering*, Oslo, Norway, Ocean, Offshore and Arctic Engineering (OOAE) Division, American Society of Mechanical Engineers (ASME International), OMAE2002-28146.
- Violante-Carvalho, N., F. J. Ocampo-Torres, and I. S. Robinson, 2004: Buoy observations of the influence of swell on wind waves in the open ocean. *Appl. Ocean Res.*, **26**, 49–60.
- WAMDI Group, 1988: The WAM model—A third generation ocean wave prediction model. *J. Phys. Oceanogr.*, **18**, 1775–1810.
- Wang, D. W., D. A. Mitchell, W. J. Teague, E. Jarosz, and M. S. Hulbert, 2005: Extreme waves under Hurricane Ivan. *Science*, **309**, 896.
- WISE Group, 2007: Wave modelling—the state of the art. *Prog. Oceanogr.*, **75**, 603–674, doi:10.1016/j.pocean.2007.05.005.
- Wu, C. H., and H. M. Nepf, 2002: Breaking criteria and energy losses for three-dimensional wave breaking. *J. Geophys. Res.*, **107**, 3177, doi:10.1029/2001JC001077.
- Young, I. R., 2006: Directional spectra of hurricane wind waves. *J. Geophys. Res.*, **111**, C08020, doi:10.1029/2006JC003540.
- , and G. P. van Vledder, 1993: A review of the central role of nonlinear interactions in wind-wave evolution. *Philos. Trans. Roy. Soc. London*, **342A**, 505–524.
- , and A. V. Babanin, 2006: Spectral distribution of energy dissipation of wind-generated waves due to dominant wave breaking. *J. Phys. Oceanogr.*, **36**, 376–394.

